PH.D DISSERTATION

RAPID ANTIBIOTIC SUSCEPTIBILITY TEST SYSTEM BASED ON SINGLE CELL ANALYSIS OF BACTERIA

단일 세균 분석 기반의 신속한 항생제 감수성 검사 시스템 개발

BY

EUN GEUN KIM

FEBRUARY 2014

DEPARTMENT OF ELECTRICAL ENGINEERING AND COMPUTER SCIENCE

COLLEGE OF ENGINEERING
SEOUL NATIONAL UNIVERSITY

PH.D DISSERTATION

RAPID ANTIBIOTIC SUSCEPTIBILITY TEST SYSTEM BASED ON SINGLE CELL ANALYSIS OF BACTERIA

단일 세균 분석 기반의 신속한 항생제 감수성 검사 시스템 개발

BY

EUN GEUN KIM

FEBRUARY 2014

DEPARTMENT OF ELECTRICAL ENGINEERING AND COMPUTER SCIENCE

COLLEGE OF ENGINEERING
SEOUL NATIONAL UNIVERSITY

RAPID ANTIBIOTIC SUSCEPTIBILITY TEST SYSTEM BASED ON SINGLE CELL ANALYSIS OF BACTERIA

단일 세균 분석 기반의 신속한 항생제 감수성 검사 시스템 개발

지도교수 권 성 훈

이 논문을 공학박사 학위논문으로 제출함

2013 년 12 월

서울대학교 대학원

전기컴퓨터 공학부

김 은 근

김은근의 공학박사 학위논문을 인준함

2013 년 12 월

위 원 장 : 박 영 준

부위원장 : 권 성 훈

위 원 : 서 종 모

위 원 : 김 성 재

위 원 : 천 홍 구

Abstract

Antibiotic resistance broke out once the first use of an antibiotic (penicillin) and has become one of the most serious problems in clinical area. There are about 750,000 patients suffering from severe sepsis each year in U.S. hospitals, and over 25 % patients do not survive. Therefore, a rapid antibiotic susceptibility test (R-AST) system is urgently needed and a quick and accurate antimicrobial therapy through R-AST is expected to reduce the rates of sepsis mortality and antimicrobial resistance.

The traditional principal, measuring optical density (OD), to observe bacterial growth is still used for over one century and it takes 16~24 hours for current AST systems based on OD to obtain AST results, which cannot cope with sepsis and antibiotic resistance properly There are several automated medical instrument related antibiotic susceptibility test in the hospital to diagnose the many patient. However, the automated AST platforms also take optical density (OD) to measure growth of bacterial population in media including different concentrations of various antibiotics and so need more than 9 hour incubation time for the differentiation between antibiotic-susceptible and resistant strains.

In this dissertation, a potentiometric flow cytometer capable of parallelization has been demonstrated for bacterial concentration measurement. And then, rapid antimicrobial susceptibility test system was implemented and verified. It is a new method to overcome the fundamental limit of the current methods. Also, rapid AST can be applied to same day treatment. This proof-of-concept analysis with morphological determination offers a rapid and accurate AST results compared with existing clinically available methods.

In this study, the rapid antibiotic susceptibility test analysis technology based on single cell analysis of bacteria was developed. Not only number of bacteria could be observed closely but also the heterogeneity of the various studies on the potential could be presented. In addition, if the technology is commercially available, it is expected that enable quick diagnosis and early response for bacterial infections such as sepsis than the conventional system and prevent the spread of multidrug-resistant bacteria due to abuse of antibiotics prevalent in the Republic of Korea.

Keywords: Antibiotic susceptibility test, Bacteria counting, Bacteria concentration, Microfluidic channel, Motorized Optical microscopy system, Clinical test.

Student Number: 2010-30977

Contents

List of Figures

List of Tables

Chapter 1

Introduction

In this dissertation, a development of rapid antibiotic susceptibility test system based on single bacteria analysis is presented. As a significant breakthrough in antibiotic susceptibility test (AST), we suggest a Rapid-AST(R-AST) system that determines minimal inhibitory concentrations (MICs) by analyzing bacterial growth imaging with a single cell resolution and reduces AST time dramatically. We proposed the two kinds of technologies capable of counting small concentrations of bacteria using microfluidic coulter counting technology and

image based single bacteria analysis system which is microfluidic agarose channel chip and motorized optical microscopy for automatic measurement and analysis.

In Chapter 2, I introduce a background of the research and the corresponding research motivation. On the basis of conventional method of antibiotic susceptibility test, the necessity of rapid antibiotic susceptibility test is presented. And to reduce the rapid antimicrobial susceptibility test time, R-AST technology will be compared with an existing technology.

In Chapter 3, the development of a microfluidic potentiometric multichannel flow cytometer is presented. Parallelized microfluidic channels sharing a fluid path inevitably suffer from inter-channel signal crosstalk that results from electrical coupling within the microfluidic channel network. By employing three planar electrodes within a single detection channel, we electrically decoupled each channel unit, thereby enabling parallel analysis by using a single flow cytometer microchip with multiple microfluidic channels. Therefore, this methodology should enable high-throughput and low-cost flow cytometry and in addition, facilitate bacteria concentration measurement.

In Chapter 4, I introduce a novel biochip fabrication technology. For single cell tracking in antimicrobial susceptibility test, we needed a micro-environment for bacterial immobilization and stable antibiotic supply. Here, microfluidic chip injection molding, micro patterning using hot embossing technology, and solvent

bonding technology will be introduced. Furthermore, for the tracking and rapid examination of single bacterial growth, the motorized optical microscopy reader system including a software was developed and used in this study. By single cell tracking method, different growth pattern of bacteria according to the relation with species and antibiotics was observed. In this study, we established a new image method that morphological change is directly related with antimicrobial susceptibility. Using this method, rapid antibiotic susceptibility test was possible.

Chapter 2

Background and Motivation

In this chapter, I introduce a background and a motivation of this dissertation. After an introduction of conventional antimicrobial susceptibility test method, the reason why we need rapid AST is referred to. On the basis of conventional method of antibiotic susceptibility test, the main goal of rapid antibiotic susceptibility test is introduced. Finally, previously-established approaches for bacteria concentrator and microfluidic AST system are presented.

2. 1 Why Rapid Antibiotic Susceptibility Test(R-AST)

Antibiotic resistance broke out once the first use of an antibiotic (penicillin) and has becoming one of the most serious problems in clinical area. Fast antimicrobial treatment demanding sepsis is one of the leading causes of death in the intensive care unit. There are about 750,000 patients suffering from severe sepsis each year in U.S. hospitals, and over 25 % patients do not survive [1]. Therefore, a rapid antibiotic susceptibility test system is urgently needed and a quick and accurate antimicrobial therapy through R-AST is expected to reduce the rates of sepsis mortality and antimicrobial resistance [2].

The traditional principal, measuring optical density (OD), to observe bacterial growth has still used for over one century and the current AST systems based on OD take 16~24 hours to obtain AST results, which cannot cope with sepsis and antibiotic resistance properly. There are several automated medical instrument related antibiotic susceptibility test in the hospital to diagnose the many patient. However, the automated AST platforms also take optical density (OD) to measure the growth of bacterial population in media including different concentrations of various antibiotics and so need more than 9 hour incubation time for the differentiation between antibiotic-susceptible and resistant strains [3].

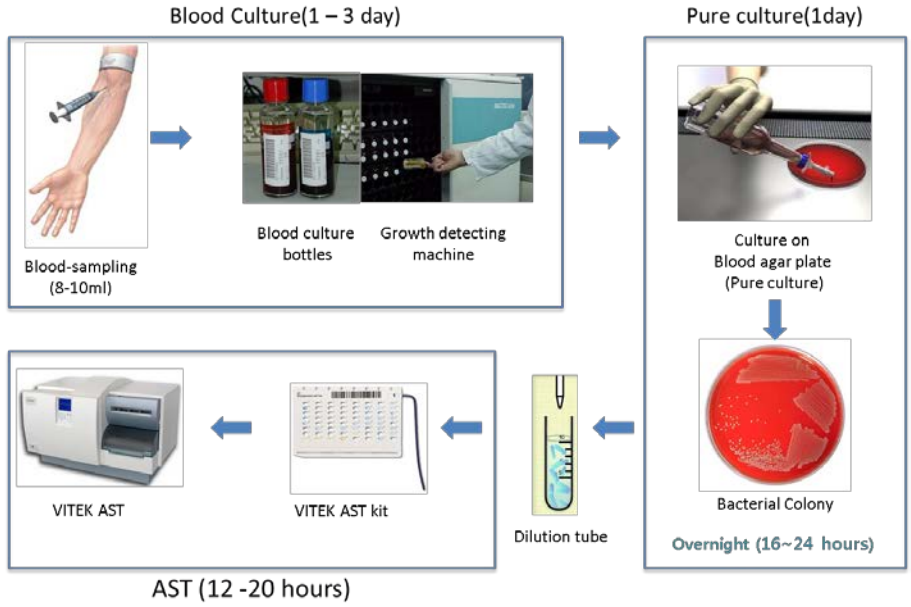

Figure 2.1 Conventional antibiotic susceptibility tests performed in the clinical process. The conventional AST platforms take optical density (OD) to measure the growth of bacterial population in media including different concentrations of various antibiotics and so need more than 9 hour incubation time.

To reduce the AST time, researchers have tried to apply new techniques. For examples, the molecular diagnosis technique is the non-incubation method to detect special antibiotic resistance genes from pathogen bacteria such as PCR and

sequencing, Matrix-assisted laser desorption/ionization time-of-flight mass spectrometry (MALDI-TOF MS), DNA microarray and so on [4]-[6]. Only few resistance genes against few antibiotics are isolated and it is very difficult to be applied in various clinical bacterial cases. The incubation method copes with almost clinical bacterial infection cases and is the most accurate. Therefore, many researchers are trying to detect bacterial growth directly or indirectly at early stage to reduce AST time with various methods. Among these methods, currently microfluidic chips are frequently used and bacterial single cell growth is observed in microfluidic chip [7]-[21]. However, it is difficult to isolate and chase bacterial growth with single cell resolution because many bacterial cells are not immobilized in this system. There is another limitation in image application. To determine antibiotic susceptibility, bacterial growth is measured simply by pixel number. However, there are many cases that expansion of bacterial volume indicates the antibiotic susceptible. For such a reason, new R-AST systems cannot be validated with various bacterial strains and has much difficulty to scale up for clinical application. In addition, those methods are mostly expensive and not ease to handle to user [22].

2. 2 The Goal of Rapid Antibiotic Susceptibility Test

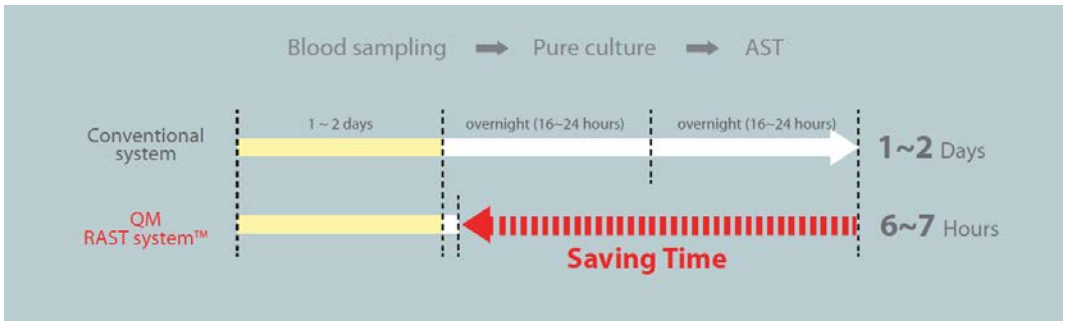

Figure 2.2 Goal of R-AST system. Comparison between conventional system and our new rapid AST system.

Figure 2.2 is shows the comparison between conventional system and our new rapid AST system. Once bacterial cells are in the blood of patients after sampling, the sample is incubated for amplification process (usually ~ 105 cells / ml or more) for 1~2 days. After then, pure culture on solid medium for a smear culture is performed under the process of the solid medium (Overnight, 16 ~ 24 hours). Therefore, in conventional AST system, the result of AST is usually up to four days for bacterial infections after sampling the blood collected from patients.

The goal of rapid antibiotic susceptibility test system is reducing AST time to 2 to 3 hours after incubation of 6-7 hours from patient blood samples. Through the image-based single bacterial cells, rapid antimicrobial susceptibility test results faster than existing methods.

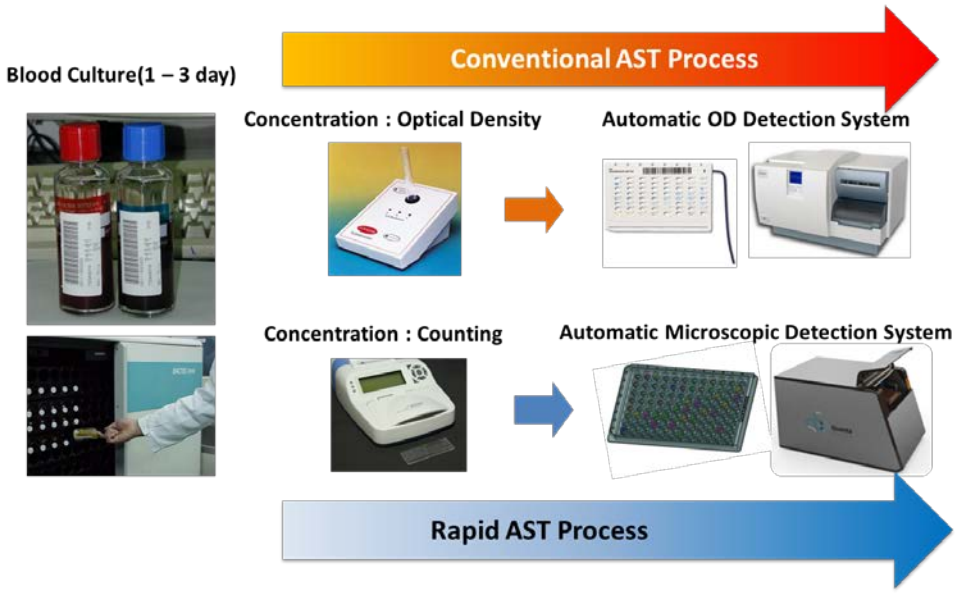

Figure 2.3 is shows that compared with conventional system and our new rapid AST system.

We hypothesized that bacterial single cell has morphological patterns to determine its susceptibility against antibiotics. By morphological analysis of bacterial cells, we could determine the drug susceptibility in few hours. In this study, we developed a microfluidic agarose channel (MAC) chip using micro-fabrication and image processing technologies for a novel R-AST system. In the MAC chip, bacterial cells were immobilized in microfludic channels integrated with conventional 96 wells for nutrient and antibiotic provision. We performed morphological analysis using our image processing program and categorized bacterial single cell growth into several morphological patterns. The minimal

inhibitory concentrations (MICs) of relevant antibiotics were determined by the morphological patterns. In proof-of-principle studies, we obtained MIC values from four standard strains of CLSI and conducted the breakpoint analysis with clinical strains. The AST results were compared with data of CLSI, golden standard and commercial AST platforms.

2. 3 Bacterial Counting for Concentration Measurement

Many studies require the quantitative determination of bacterial populations. The several methods for determining bacterial numbers are the plate count method for vial bacteria counting and spectrophotometric analysis, Mcfarland method, coulter counting method for total bacteria counting. The standard plate count method consists of diluting a sample with sterile saline or phosphate buffer diluent until the bacteria are dilute enough to count accurately. That is, the final plates in the series should have between 30 and 300 colonies. Fewer than 30 colonies are not acceptable for statistical reasons (too few may not be representative of the sample), and more than 300 colonies on a plate are likely to produce colonies too close to each other to be distinguished as distinct colony-forming units (CFUs). The assumption is that each viable bacterial cell is separate from all others and will develop into a single discrete colony (CFU). Thus, the number of colonies should give the number of bacteria that can grow under the incubation conditions employed. A wide series of dilutions (e.g., 10^{-4} to 10^{-10}) is normally plated because the exact number of bacteria is usually unknown. By using a spectrophotometer, the amount of transmitted light decrease as the cell population increases. The transmitted light is converted to electrical energy, and this is indicated on a galvanometer. The reading, called absorbance or optical density, indirectly reflects

the number of bacteria. This method is faster than the standard plate count but is limited because sensitivity is restricted to bacterial suspensions of 10^7 cells or greater [23].

A Coulter counter is an apparatus for counting and sizing particles suspended in electrolytes. It is used for cells, bacteria, prokaryotic cells and virus particles. A typical Coulter counter has one or more microchannels that separate two chambers containing electrolyte solutions. As fluid containing particles or cells is drawn through each microchannel, each particle causes a brief change to the electrical resistance of the liquid. The counter detects these changes in electrical resistance [24], [25].

Spectrophotometric, Mcfarland and Coulter Counter method cannot distinguish between living and dead bacteria, which determine the total bacterial concentration. If size and count data are needed for just the living bacteria, the analysis has to be backed up by assessment of cultures in petri dishes, or some other technique, to find out what percentage of the bacterial population is living.

2.4 Microfluidic based Antibiotic Susceptibility Test

To reduce the AST time, microfluidic channel systems for R-AST have been developed recently [5]-[15]. The microfluidic chip provides several advantages in terms of reducing the AST time by using of small quantities of samples and reagents, high detection sensitivity, and reduced analysis time [16],[17]. Chen et al.6 used the large surface-to-volume ratio of polydimethylsiloxane (PDMS) microfluidic systems to rapidly detect the growth of bacteria. In the droplet-based microfluidic channel system, bacteria were captured in one droplet that included an antibiotic for AST [5],[12]. In another droplet system, agarose microparticles for encapsulating bacteria and fluorescence activated cell sorting were used for R-AST [7]. For faster MIC determination, an asynchronous magnetic bead rotation biosensor was invented for R-AST [11]. These methods are based on detecting indirect signals caused by changes in the bacterial cell population due to multiple cell divisions, which is similar to conventional AST methods.

Bacterial cell division normally takes about 20–40 min. Direct observation of the doubling of single bacterium cell in bacterial population would enable the ultimate reduction in AST time. It is of interest to obtain time lapse images of single bacterial cell in test cultures. Although a microfluidic chamber confines bacteria to a small volume, they still move and float in the media, thereby making

it difficult to track single bacterial cells and obtain time lapse images. To enable R-AST based on single cell imaging, it is necessary to fix the bacteria. To immobilize motile bacteria in a microfluidic channel, the dielectrophoresis (DEP) method was employed, and bacterial single cell growth against an antibiotic was monitored by using time lapse microscopy [9]. Although an MIC result can be obtained in 5 h by using this system, the inoculum effect and DEP force affects its accuracy. Using this system, it resulted in an MIC that is one order of magnitude less compared with the MIC value obtained by using a conventional system. Therefore, a more reliable bacterial cell immobilization method that does not influent bacterial cell growth is needed for R-AST.

Chapter 3

Bacteria Concentration Measurement

3. 1 Introduction

Flow cytometry is an analytical methodology in which optical and/or electrical detection are used to determine various characteristics of individual samples flowing through the detection region. By providing quantitative analysis result, the application of flow cytometry enables analysis of various sample characteristics ranging from the basic material properties of biological and

nonbiological particles to the complicated physiological and biochemical characteristics of cellular processes[26]-[28].

Clearly, flow cytometers have a wide range of applications; however, currently available flow cytometers are cost- and labor-intensive. Furthermore, the entire cytometry system, including the peripheral equipment, is quite bulky and complicated, making the use of flow cytometry inappropriate to point-of-care test for the global health. Advancements in microfabrication technology have led to the development of lab-on-a-chip technology, and this in turn has facilitated attempts to miniaturize flow cytometers in order to achieve portable and disposable point-of-care test devices. Thus far, many studies have endeavored to develop various types of micromachined flow cytometers, and these studies have made remarkable progress in the context of reduced size and cost of flow cytometry [29]-[34].

With regard to the development of miniaturized flow cytometers, electrical detection, which is used to analyze the translocations of an analyte through a channel or an aperture based on conductivity measurement, has been considered advantageous compared to optical detection owing to its simpler configuration and lower cost [35]-[40]. Among recent developments in electrical detection, a high-throughput nanoparticle analyzer, a multifunctional size-adjustable nanopore device, and nanopore devices for single DNA molecule analysis have been demonstrated to have great potential for advanced nanoscale applications [41]-[50].

In addition to simple sizing and counting applications based on the Coulter principle, micromachined devices with an elaborate electrode arrangement can be applied to studies of complex cellular characteristics through impedance analysis [51]-[55].

Despite its ability to realize quantitative cell analysis and with the progress being made toward its miniaturization, flow cytometry suffers from an inherent trade-off between the throughput and the sensitivity of analysis. In addition, recent times have witnessed an increased demand for biological and clinical screening applications, including multiplexed drug screening. To address issues pertaining to the throughput, sensitivity, and screening, studies are now focusing on the parallelization of flow cytometers. For example, McKenna *et al.* developed a parallel flow cytometer that combines multiple microfluidic channels and one-dimensional imaging configurations [56], [57]. Hur *et al.* utilized a multichannel parallel microfluidic device under the influence of inertial ordering effects to achieve extremely high throughput (~10^6 cells s^{-1}) blood cell counting [58]-[61]. While these methods show highly improved multiplexity or throughput, respectively, they require a bulky and expensive optical detection system that includes a confocal scanner or a high-speed camera. Parallelized Coulter counter devices employing multiple detection channels have also been demonstrated. A major difficulty in parallelization is that coupled electric circuits comprising

multiple channels connected via electrolyte filling inevitably suffer from interchannel signal crosstalk that hinders independent detection. Jagtiani *et al.* prevented signal crosstalk by placing each channel unit separately or by allowing each detection channel to carry its signal on a unique carrier frequency [62]-[64]. However, these approaches are practically inappropriate for miniaturization or the sampling rate, i.e., detection throughput, is limited by the increase in the number of channels sharing the limited bandwidth.

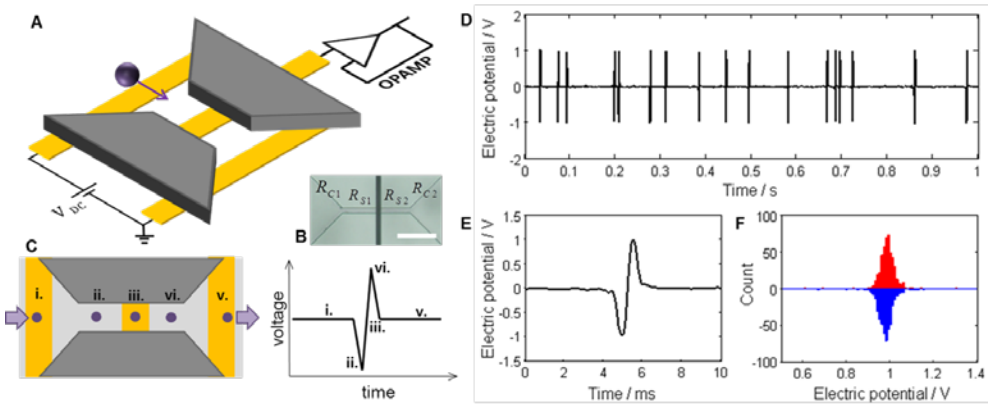

Figure 3.1 Potentiometric flow cytometer. (A) A schematic view of the device, which has three planar electrodes and a sensing channel. (B) A micrograph of a fabricated sensing channel with a sensing electrode at the middle. Scale bar indicates 50 μm. (C) A step-wise descriptive view of the electric potential change during microbead translocation. (D) A representative electric potential trace obtained by a sensing electrode (after filtering and noise reduction). (E) Enlarged view of a single translocation

signal. (F) Amplitude distribution of peaks and valleys obtained from a typical electric potential trace. A microbead suspension with bead diameter of 2.58 μm was used in (D)–(F).

In this study, we report a micromachined potentiometric flow cytometer capable of parallelization [65]. The microchip comprises three electrodes—a pair of voltage-applying electrodes and one sensing electrode between them—within a single electrolyte-filled microfluidic channel (Figure 3.1 A). In the triple-electrode configuration, the inner part of the microfluidic channel (i.e., sensing channel) forms a closed electric circuit with the voltage-applying electrode pair whereas the outer part has no external electric connections. Therefore, the electric resistance distribution within the sensing channel is only subject to change under intrachannel events such as translocations of microbeads having a size comparable to the dimensions of the sensing channel. In particular, when a sensing electrode is situated at the middle of the voltage-applying electrode pair, which maintains a constant potential drop across the sensing channel, the electric potential read responds to the translocation of a single microbead by showing biphasic and symmetric potential pulses, enabling analysis of the samples of interest. We first validated the applicability of our approach to flow cytometry. By using the triple-electrode configuration, we analyzed microbead suspensions having various sizes

and concentrations. We then applied our device to the study of biological particles—in particular, bacterial suspensions—and demonstrated its potential for use in biological and medical applications. With regard to bacterial suspensions, we estimated and differentiated various bacterial concentration ranges lower than 1×10^7 CFU mL^{-1}, in which the concentration differences of bacterial suspensions are indistinguishable based on a conventional microdilution antibiotic susceptibility test. By exploiting the fact that a single detection channel is electrically isolated from its surroundings, our approach can be easily expanded to a single flow cytometer with multiple channel units. To achieve parallelized high-throughput analysis, we demonstrated a potentiometric flow cytometer microchip with 16 detection channel units sharing a fluid path. The detection throughput of our method can be easily increased without loss of sensitivity by simply increasing the number of detection channel units in the microchip.

3. 2 Materials and Methods

3.2.1 Reagents

All reagents were purchased from Sigma Aldrich (St. Louis, MO) unless otherwise specified. Polystyrene microbeads (NIST Traceable Particle Size Standard, 2 μm, 2.5 μm, 3.5 μm, and Sure Count Particle Count Standards, 3 μm) were purchased from Polysciences (Warrington, PA). The culture broth (Muller Hinton II Broth Cation Adjusted) was purchased from Becton, Dickinson and Company (Shannon, Ireland).

3.2.2 Microchip Fabrication

By assembling and bonding two glass substrates—one with a microfluidic channel and the other with an electrode pattern—a single-channel or multichannel device was fabricated. The microfluidic channel substrate was prepared by the dry etching of a glass substrate. First, an etching mask was formed on a glass wafer through photolithography, aluminum deposition (1 μm), and lift-off in sequence. The aluminum layer for etch inhibition was deposited on the backside of the wafer, following which glass dry etching was performed to form a microfluidic channel. The length, width, and height of the sensing channel were measured to be 100, 7,

and 10 μm, respectively (Figure 1B). After aluminum removal and substrate cleaning, inlet/outlet access holes (diameter: ~1 mm) were drilled by sandblasting. An electrode substrate was prepared so as to have a flat and conformal bonding surface without electrode protrusion. To do so, first, we prepared a photoresist mask pattern on a glass wafer through photolithography and formed a trench structure with a depth of ~110 nm by soaking the wafer in buffered oxide etchant solution for a short duration. The electrode was then formed through the deposition of 10 nm/100 nm Ti/Pt using an e-beam evaporator, following which a lift-off process was performed to obtain a planar electrode within the trench structure. A flat glass bonding surface was provided by matching the trench depth to the electrode height. The two substrates were finally bonded together by using a direct bonding technique. Briefly, the substrate surfaces were hydrolyzed in $NH_4OH/H_2O_2/H_2O$ (2:1:2) solution at 70°C for 30 min. After rinsing with deionized water, the substrates were aligned and joined, and then annealed at 300°C for 10 h. All fabrication steps except for substrate alignment and bonding were carried out at the Korea Bio-IT foundry center.

3.2.3 Sample Preparation

The initial concentration of the microbead suspension was calculated in consideration of its weight fraction (1 % w/v), density of polystyrene (1.05 g cm^{-3}),

and volume of a single microbead. Microbead samples with desired concentrations were prepared by diluting the source suspension with 10 mM phosphate buffer at pH 7. The concentration of a microbead sample with a diameter of 3 μm was 1×10^6 mL^{-1} as delivered. To prepare a suspension with higher concentrations, the microbead suspension was centrifuged at 13500 rpm (CF-10, Wisespin) for 2 min followed by supernatant removal and re-suspension in the phosphate buffer.

A suspension of *Bacillus Subtilis* previously stored at -65 °C was defrosted and cultured in 10 mL broth inside an incubated shaker (SI-600R, JEIO Tech.) at 37 °C for 12 h. Based on the optical density measurement at a wavelength of 600 nm, the concentration of the bacterial suspension was adjusted to be approximately 1.48×10^7 CFU mL^{-1} by diluting in the culture medium by referring to the McFarland Standards.[45] The bacterial suspension in the phosphate buffer was prepared through bacteria separation using a centrifuge (5000 rpm, 2 min), intermediate pellet washing, and re-suspension in the phosphate buffer in sequence. The final bacterial suspension was successively diluted in the same buffer to obtain a series of bacterial suspension samples with different concentrations.

3.2.4 Single Detection and Data Acquisition

The microfluidic channel of a device was filled with 10 mM phosphate buffer at pH 7. The outlet of the device was then connected to a flexible tube (Tygon

microbore tubing 0.02" × 0.060", Cole-Parmer) coupled with a disposable plastic syringe. A syringe pump (PHD Ultra, Harvard Apparatus) generated a constant flow of 10–500 μL hr^{-1} after sample loading into the inlet of the device. While the voltage-applying electrodes maintained a constant potential drop across the sensing channel, the electric potential obtained by the sensing electrode was passed to a custom analog filter circuit. In order to filter the DC component and amplify small electric potential variations, a high-pass filter with a cut-off frequency of 0.5 Hz was used in combination with a two-stage operational amplifier (amplitude gain: ~1600, low-pass filter cut-off frequency: ~10 kHz). The filtered electric potential traces were acquired using a data acquisition board (NI USB-6212, National Instruments) at a sampling rate of 24 kHz for each channel.

3.2.5 Data Analysis

Data analysis was performed using a custom script written in LabVIEW (National Instruments) and MATLAB (MathWorks). The obtained electric potential trace was first processed using a wavelet denoise filter in the discrete wavelet transform mode. The threshold electric potential change for signal identification was chosen as a signal-to-noise ratio (SNR) of 5. A mode potential change value was chosen as a representative potential change for each measurement with a signal acquisition time of 15 or 30 s. To estimate the

concentration of the given microdispersion samples, the number of signals within a time period of 30 or 60 s was measured at a fixed flow rate.

3. 3 Results and Discussion

3.3.1 Device Operation

The potentiometric flow cytometer unit consists of three planar electrodes and a microfluidic channel filled with electrolyte to form a closed electrical circuit. The microfluidic channel includes a sensing channel (length: ~100 μm) with higher electrical resistance than its surroundings, through which a single microbead or bacterium is allowed to translocate. To identify and analyze translocation events through the sensing channel, a sensing electrode monitors the electric potential variation at the middle of the channel while the other two electrodes lying outside the channel apply a constant potential drop across the channel.

The electric potential at the sensing electrode is mainly dependent on the distribution of the electrical resistance across the microfluidic channel:

$$V = \frac{R_{S2} + R_{C2}}{R_{C1} + R_{S1} + R_{S2} + R_{C2}} V_{DC}$$

where R_{S1} and R_{S2} are the electrical resistance on either side of the sensing electrode within the sensing channel and R_{C1} and R_{C2} are those outside the sensing channel (Figure 3.1 B). Owing to the dimension of the sensing channel being

comparable to the microbead size, R_{S1} and R_{S2} change much more sensitively than do R_{C1} and R_{C2} under microbead translocation events. Therefore, as a microbead translocates through the sensing channel, the electric potential at the sensing electrode increases ("valley") and decreases ("peak") relative to a baseline potential, showing a biphasic and symmetric potential trace (Figure 3.1 C–E). We also confirmed that a single microbead translocation event generated a single biphasic potential change through a comparison with synchronized high-speed camera images (data not shown). Figure 3.1 F shows the amplitude distribution of peaks and valleys in the biphasic translocation traces. As expected, these peaks and valleys showed equal amounts of potential changes when the sensing electrode was located at the middle of the sensing channel. In this study, the peak-to-valley amplitude differences are selected as representative translocation signals.

3.3.2 Analysis of Microbead Suspension

To validate the applicability of the triple-electrode configuration to flow cytometry applications, we analyzed suspensions of microbeads having different sizes and concentrations. Four different sizes of microbeads were analyzed using our device and shown to generate biphasic potential traces with a clearly distinguishable amount of potential change (Figure 3.2 A)—the average potential changes for microbeads with diameters of 1.99, 2.58, 3, and 3.68 μm were 0.81,

2.01, 3.16, and 5.93 V, respectively. The sizes of microbeads are also traceable from the electric potential variations obtained for a mixture of microbeads having different sizes (Figure 3.2 B). Under our experimental conditions, the amount of potential change induced by microbead translocation is found to be mainly proportional to the microbead volume (Figure 3.2 C).

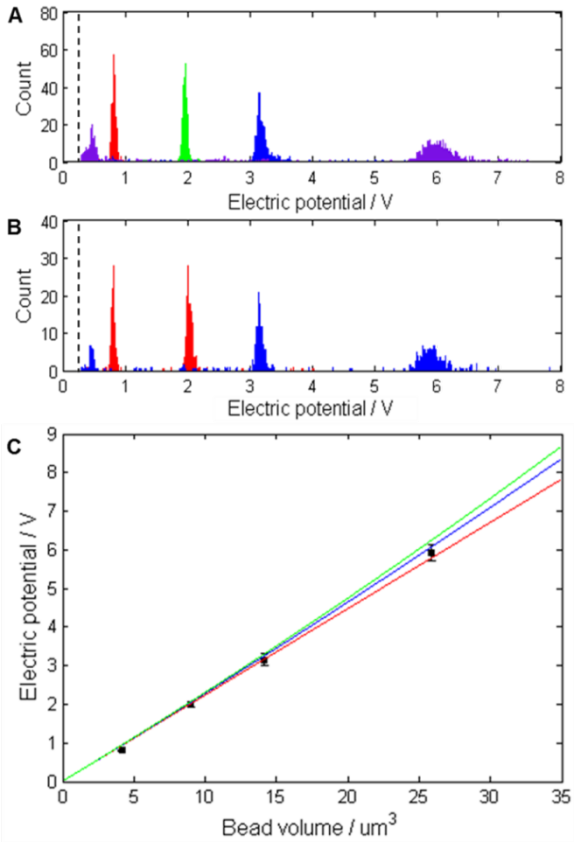

Figure 3.2 Analysis of electric signal changes induced by microbead translocations. (A) Amplitude distribution of potential changes for

microbeads with four different sizes — Red: 1.99 μm (N = 344), Green: 2.58 μm (N = 383), Blue: 3 μm (N = 386), and Violet: 3.68 μm (N = 371). (B) Amplitude distribution of potential changes for 1:1 mixtures of microbeads with two different sizes — Red: 1.99 and 2.58 μm (N = 336) and Blue: 3 and 3.68 μm (N = 371). Dashed lines indicate the threshold electric potential change. Peaks near 0.43 V are generated by the translocation of small satellite microbeads (diameter: ~1.61 ± 0.14 μm) included in the suspension of microbeads having a diameter of 3.68 μm (confirmed by scanning electron microscopy imaging). (C) Relation between volume of microbeads and corresponding electric potential changes. Curves indicate estimated potential changes based on various theoretical models — Red: Maxwell theory, Blue: Smythe model, and Green: Deblois model.

In addition to the measurement of the microbead size (or volume), our device can also be used to estimate the concentration of microbead suspensions. The capability for measuring the microbead concentration as well as the size distribution is essential for a flow cytometer device from the viewpoint of enabling the quantitative analysis of samples of interest in various research fields. The concentration of microbead suspensions can be calculated from the microbead

count rates as follows:

$$J = C(Q + S \cdot \frac{\mu}{l} V)$$

where J is the microbead count rate; C, the concentration of the microbead suspension; Q, the volumetric flow rate inside the sensing channel; μ, the electrophoretic mobility of the microbeads; and V, the electric potential drop across the sensing channel (diffusion ignored); furthermore, S and l are the cross-sectional area and the length of the sensing channel, respectively [21]. Here, the effect of electro-osmosis can be ignored by the use of a syringe pump maintaining a constant flow rate. Because the microbeads used in this work are electrically neutral, the electrophoretic movement of microbeads is also expected to be negligible. With the considerations discussed above, the estimated concentration of the microbead suspension was simplified as the microbead count rate divided by the volumetric flow rate inside the sensing channel. Figure 3.3 shows the concentration estimation result for several microbead suspensions with various concentrations. In this study, we chose the concentration range of ~2×10^5 mL^{-1} to 1×10^7 mL^{-1}, which is as low as the initial concentration range of bacteria test samples for the microdilution antibiotic susceptibility test (see next part — Analysis of bacteria suspension).

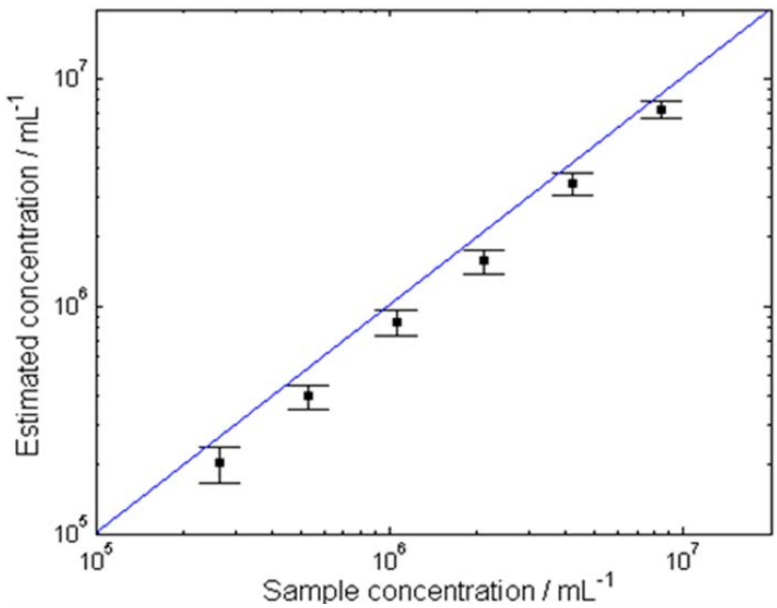

Figure 3.3 Concentration estimation of microbead suspensions (N = 3). The line in the plot indicates the ideal line with estimated concentrations equal to sample concentrations. Microbead suspensions (diameter: 2.58 μm) of various concentrations were used.

By using our device, we could estimate and clearly distinguish the concentration of microbead samples prepared by successive dilutions (N = 3, CV: ~11.5 % on average). For all concentrations investigated, we found a common underestimation of 19.1 ± 3.6 %. We attributed this underestimation of the sample concentration to the miss estimation of the flow rate inside the sensing channel caused by the use of flexible pneumatic parts (a syringe and a tube). The

underestimation could also be attributed to the exclusion of bead dimer (or two neighboring beads) counts or sample loss caused by bead adhesion to the channel wall. In all measurements, however, the count of bead dimer translocations, which are expected to generate potential traces with double the potential change, was extremely low and negligible. Furthermore, we could hardly see microbeads remaining on the channel wall after the measurement. The estimation accuracy will increase further if pressure-resistant elements are used. The results of microbead analysis, including size measurement and concentration estimation, are summarized in Table 3.1.

Table 3.1 Analysis of microbead suspensions with various sizes and concentrations. Provided by manufacturer (No information for microbeads with diameter of 3 μm).b Error [%] = ((signalbead/signal2.5μm) − volume)/volume × 100.c Used as a reference for size error calculation. d Expected sample concentrations (prepared by dilution of source samples as purchased). e No estimation result due to microbead clogging at the filter post array inside a device.

sample	diameter[a] [μm]	signal [V] (N > 40)	CV [%]	sample concentration[d] [10^6 mL^{-1}]	estimated concentration [10^6 mL^{-1}]	CV [%]	error [%]
2 μm	1.99±0.06	0.809±0.016	2.0	2.31×10^6	2.18 ± 0.25	11.6	5.3
2.5 μm	2.58 ±0.06	2.009±0.068	3.4	2.11×10^6	1.93 ± 0.29	14.9	8.5
3 μm	3	3.159±0.160	5.1	2×10^6	1.78 ± 0.12	6.7	11.0
3.5 μm	3.67±0.13	5.925±0.215	3.6	2.19×10^6	-[e]	-	-

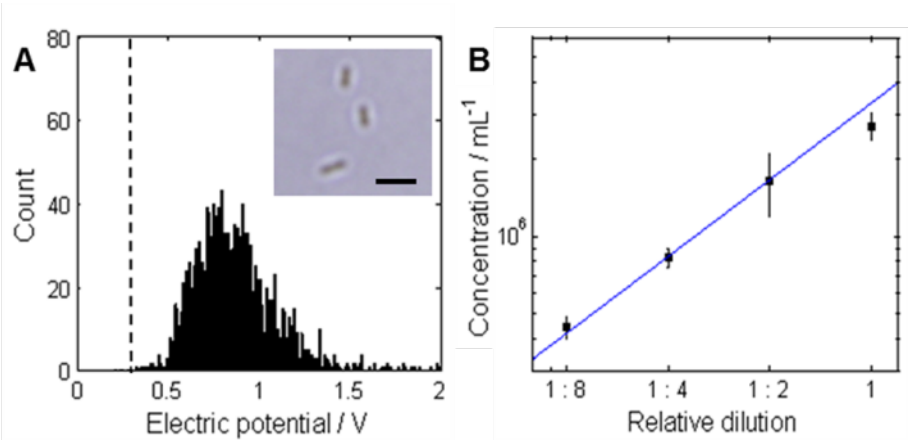

Figure 3.4 Analysis of bacteria suspension. (A) Amplitude distribution of potential changes induced by translocations of Bacillus subtilis. Inset

shows a micrograph of Bacillus subtilis. The scale bar indicates 10 μm. (B) Concentration estimation of bacteria suspensions with various dilutions (N = 3). Relative dilution of 1 corresponds to an estimated sample concentration of 1.85 × 106 CFU mL-1, which was prepared by diluting a source suspension with an estimated concentration of 1.48 × 107 CFU mL-1 based on optical density measurement. The line in the plot indicates an empirical trend line obtained from measured concentrations.

3.3.3 Analysis of Bacteria Suspension

By using the microbead analysis result as a calibration standard, we analyzed the size and concentration of the bacteria suspension samples. We chose *Bacillus subtilis* as our model bacteria because its size is comparable to that of the microbeads analyzed in this study. Various bacteria other than *Bacillus subtilis* can also be analyzed using the same device with appropriate channel dimensions. The average potential change for the translocations of *Bacillus subtilis* is obtained to be 0.79 V, which corresponds to an estimated volume of 3.53 μm^3. This value is in good agreement with the typical dimension of *Bacillus subtilis* (diameter: ~1 μm, length: ~4 μm) [66]. Figure 3.4 A shows a representative potential change distribution for *Bacillus subtilis*; it has a wider distribution than the microbead suspensions. We interpret the large distribution (0.5–1.3 V) as the inherent size range of bacteria samples, in which each individual bacterium lies in a different stage in the bacterial cell cycle. In addition, the nonspherical shape of *Bacillus subtilis* should contribute to this variation. Counting the number of bacteria has critical implications for various applications such as pathogenic bacteria detection in food or an antibiotic susceptibility test [67], [68]. In particular, in the latter, bacterial growth rates under exposure to various antibiotics conditions are used as bases for the selection of antibiotics with an appropriate dose. A conventional

microdilution antibiotic susceptibility test estimates and monitors the concentration of bacteria by measuring the optical density, that is, light absorption, of growing bacteria samples. The initial bacteria concentration of a standard test sample is ~5 × 10^5 CFU mL^{-1}. However, the conventional method is only capable of detecting the growth of bacteria in the bacterial concentration range above the detection limit of optical density measurement (~1 × 10^7 CFU mL^{-1}), and therefore, it requires a long incubation time before the proper antibiotic condition can be determined [23]. In this study, we investigated the concentration-estimating ability of our device by using bacteria suspensions with concentration ranges lower than 1 × 10^7 CFU mL^{-1}, in which the concentration differences between the samples were indistinguishable using optical density measurement. In Figure 4B, the concentrations of bacteria suspension samples with concentration ranges of 4 × 10^5 CFU mL^{-1} to 3 × 10^6 CFU mL^{-1} are clearly distinguished (N = 3, CV: ~14.2 % on average), suggesting that our device can potentially be used for the early identification of bacterial growth.

3.3.4 Parallelization

With the parallelization of the measurement, fluidic and corresponding electrical connections between the adjacent channels are inevitable [40]. This coupling leads to signal crosstalk and it hinders parallel and independent measurements. In contrast, because the electric potential distribution between the

two voltage-applying electrodes is set and maintained to a constant level regardless of the fluidic coupling with the neighboring channels, the sensing electrode in our device can recognize variations of electrical resistance only within the sensing channel it lies in. Consequently, our triple-electrode configuration electrically isolates individual detection channels, thus simplifying the crosstalk-free parallelization of the device into a simple multiplicative expansion of single identical detection units.

To demonstrate the crosstalk-free parallelization of our device, a potentiometric cytometer with 16 parallel detection units was prepared (Figure 3.5). Figure 3.5 B shows the 16 electric potential traces simultaneously obtained by a single 16-channel potentiometric cytometer microchip. All the detection channel units share a fluid inlet and/or outlet and are therefore electrically coupled to each other along a fluid channel, possibly with interchannel signal crosstalk during the measurement. However, because the voltage-applying electrode pairs lie within each channel unit, the potential traces show no crosstalk (Figure 3.5 C and D). We also confirmed that no signal crosstalk was found in the same experiment using Bacillus subtilis.

The detection throughput of our device can be simply determined as the throughput of a single detection unit multiplied by the number of detection units. From the analysis of the transit time distribution of translocation events, the

experimental detection throughput of a single detection channel unit was determined to be ~3000 s^{-1} without further device optimization such as a decrease in the length of the sensing channel. Therefore, the total throughput of the single 16-channel device was achieved to be ~48000 s^{-1}, which is as high as that of commercialized flow cytometers. The detection throughput can be further increased by adopting various technical approaches such as the use of polymer electrodes. Finally, the detection throughput of our device increases proportionally with the number of detection channel units in a parallelized manner, and therefore, the throughput can be increased without additional technical complexities.

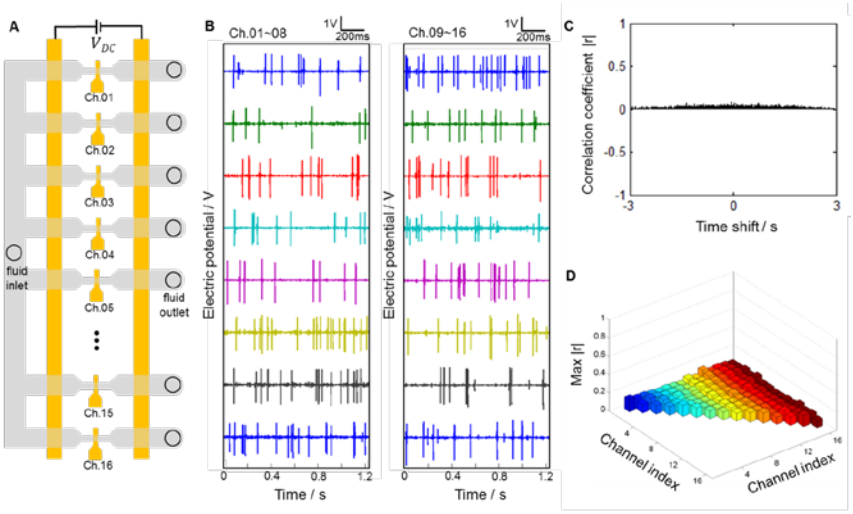

Figure 3.5 Parallelized detection of microbead translocations using a 16-channel flow cytometer. (A) A schematic view of the device with 16 detection channel units. (B) Electric potential traces simultaneously

obtained by 16 individual channels. Asymmetric shapes of the potential changes in some channels are generated due to misalignment of sensing electrodes caused by manual assembly of our device. (C) Cross-correlation analysis of the electric potential traces obtained from channels 08 and 09. (D) Maximum cross-correlation coefficients obtained from all electric potential trace combinations ($|r| < 0.13$). .

Chapter 4

Rapid Antibiotic Susceptibility Test (R-AST) System

This chapter introduces a novel biochip fabrication technology. For single cell tracking for antibiotic susceptibility test, we needed a micro-environment for bacterial immobilization and stable antibiotic supply. Here, we report the microfluidic based biochip in which surface tension and controlled flooding in laterally open channels allows for antibiotics diffusion. The use of capillary action, as opposed to active pumping, is attractive because it does not require addition of

tubing or use of a syringe pump. Therefore, it is compatible with simple pipetting.

For bacterial immobilization, liqud state agarose was mixed with bacterial strains and the mixture was pipetted into the inlet of the microfluidic channel engaged with the well supplying liquid medium including an antibiotic. One part of the antibiotic well was open into the microfluidic channel. The microfluidic channel was plasma-treated for hydrophilic so the bacteria and agarose mixture was filled in the microchannel forming an interface with the antibiotic well by capillary valve effect and the mixture did not burst into the antibiotic well (Figure 4.1) [69], [70].

After bacterial immobilization and antibiotic supply, bacterial cells on the bottom are detected based on the focusing mark carved under the film using optical reader system. Thorough the microscopic images, we can analyze the growth pattern of bacteria under the antibiotics. In this chapter, microfluidic chip injection molding, micro-patterning using hot embossing technology, solvent bonding technology will be introduced to implement MAC chip,. Moreover, the motorized optical microscopy reader system including a software was developed and used in this study for the tracking and rapid examination of single bacterial growth.

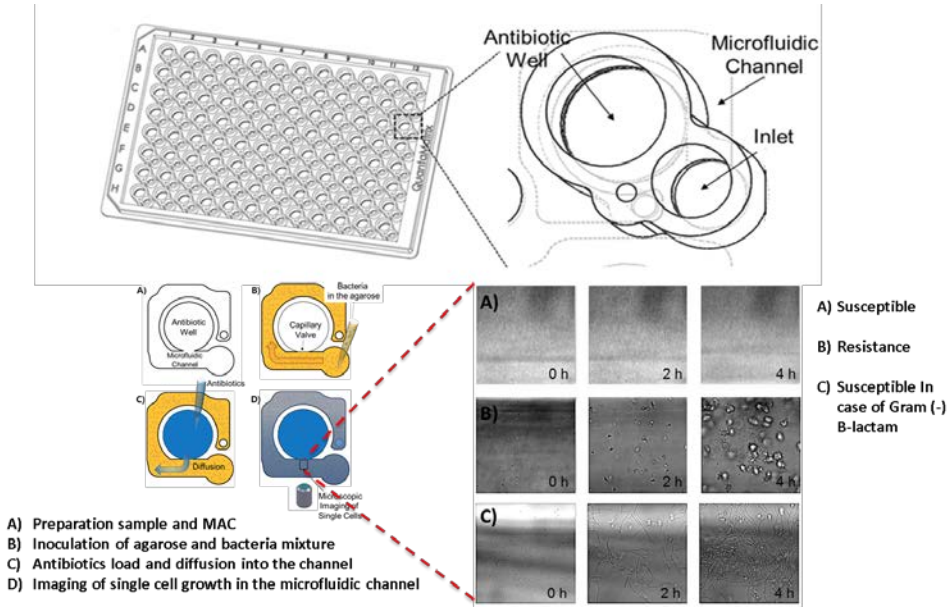

Figure 4.1 Microfluidic agarose chip principle. Liquid state agarose was mixed with bacterial strains and the mixture was pipetted into the inlet of the microfluidic channel engaged with the well supplying liquid medium including an antibiotic.

4.1 Microfluidic Agarose Channel(MAC) Chip

4.1.1 Microfluidic Chip Manufacturing

Microfluidic agarose channel chip was designed as 96 well plate which is a type of Society for Biomolecular Science (SBS) format. The structure of developed well plate is shown in Figure 4.2. There are a total of three holes in one of the well. One are injected into bacteria, which mixed with the agarose well and 2nd one is use of venting the air, the biggest one is use of injection of the antibiotic. Agarose channel for loading bacteria is 300um height, and designed allowing 10ul volume of agarose using pipette because of its high viscosity. Antibiotics are total 100ul within a size that can be injected it was composed of a micro-channel is in an area of 34.4mm^2. There is no difficulty in agarose injection inlet size of about 3mm in diameter. The microfluidic chip is designed for the injection molding of the part of the mold design. Designed microfluidic agarose chip was manufactured in injection molding company. Figure 4.2 shows the photography of injection molded MAC chip. It is made of polycarbonate. In case of QDM (Quick Delivery Mold), it can be made up to a maximum of 3000 pieces.

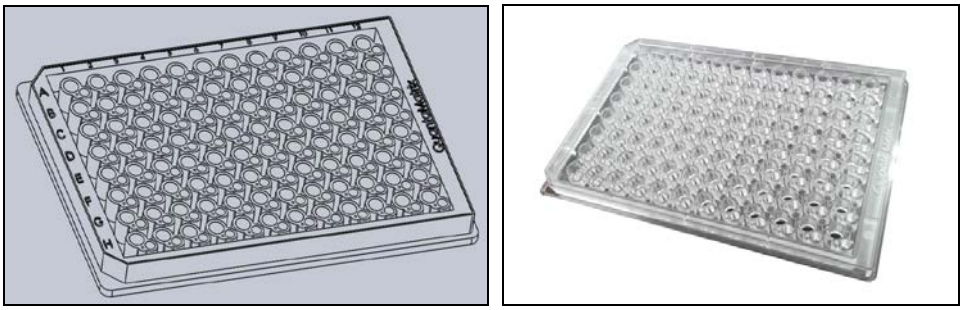

Figure 4.2 3D cad design of MAC chip, Antibiotics Well Size is 19.6mm^2, 100ul, Inlet Diameter is 3mm, Area of loading microchannel is 34.4mm^2, Channel Height is 300um, Channel Volume is 10uL. Injection molded microfluidic agarose channel plastic chip. It is made of polycarbonate.

4.1.2 Micro Patterning for Focusing Mark

PMMA (polymethylmetaacrylate) film with 0.8 mm thickness is attached to the bottom surface of the plastic well plate. The nature of the injection of thermoplastic plastic, shrinkage and flexure are generated, so that significant error effect results in magnification of the microscope. To overcome this problem, micro patterned focusing mark is needed at the observation region in each well. Focusing mark is carved on the bottom side of the film using hot embossing method.

Nickel stamper were fabricated for use as hot embossing mold. 6-inch bare Si(100) wafer was prepared for the hot embossing mold. A layer of positive photoresist was spin-coated at 3000 rpm for 30 seconds. The coated photoresist had a 1 μm thickness and was baked on a hot plate at 100°C for 1 minute. The surface was exposed by means of a UV Aligner through a photomask and the photoresist was developed. The patterned photoresist wafer was dry-etched in deep RIE to make a Si mold and photoresist strip was performed. For an optimal release process between the mold and replica, an antistiction layer was coated on the mold prevent electroplated nickel stamper. 5nm thickness of anitistiction layer was deposited by deep Etcher using a C_4F_8 gas. After then, nickel seed layer of 50nm was deposited for electroplating. This silicon mold fabrication step was carried out at the Inter-university Semiconductor Research Center (ISRC, South Korea). Nickel film was

electroplated with a plating bath and a chemical nickel electrolyte was used for the electroplating of Ni to make Ni stamp. Backside lapping and dicing process was performed and carried out at DS Semicon (South Korea). This nickel stamper fabrication process is shown in Figure 4.3

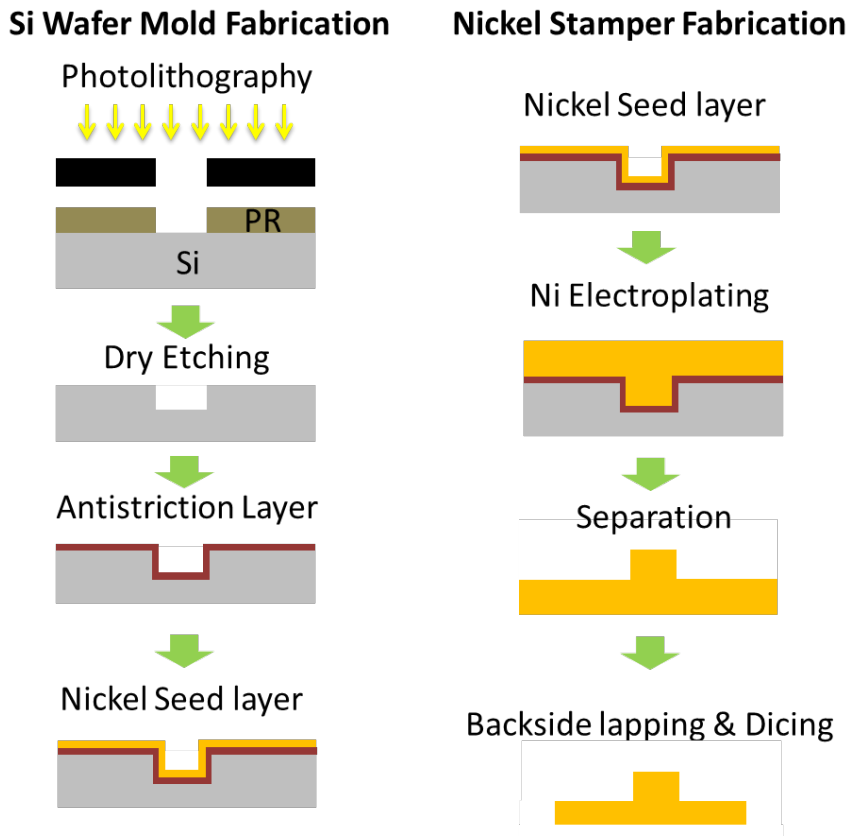

Figure 4.3 Si wafer fabrication (Photolithography-Dry etching-Antistriction layer-Nickel seed layer) and Nickel electroplaiting fabrication(Electroplating-separation-Backside lapping and Dicing).

PMMA (polymethylmetaacrylate) film with 0.8 mm thickness was purchased from Sejin TS (Korea) to make replica of a stamp substrate. Imprinting was performed in a hot embossing (Internally developed Equipment. The fabricated nickel stamp was carefully mounted into a clamp and sandwiched with a PMMA film. The hot embossing process was achieved a functions of both temperature and pressure - the weight was 1000kg, the temperature was 90 °C, and the process time was 5 min. Figure 4.4 shows internally developed hot embossing machine. Using servo press, positioning accuracy and uniformity of the load was increased than pneumatic or hydraulic pressure equipment. Figure 4.5 shows a photograph of an imprinted result on a 0.8 mm PMMA substrate. After the imprinting process, all of the patterned structures were observed by an optical reader system. A various thickness of PMMA film can be used for optimizing hot embossing process. The thickness of focusing mark pattern is about 800nm. The size error between Ni mold and PMMA is about 200um. It is caused by the thermal expansion coefficient difference and the bubble between the film and stamper(Figure 4.6).

Figure 4.4 Developed hot embossing machine. This machine consists of servo press, wafer loading jig, two hot plates, and control PC.

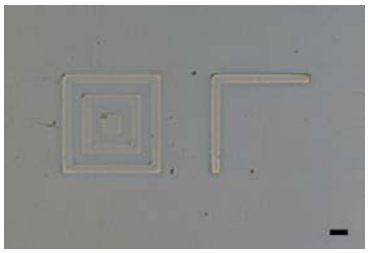

Figure 4.5 Photograph of an imprinted result on a 0.8 mm PMMA substrate when the weight was 1000kg, the temperature was 90 ℃, and the process time was 5 minutes.(Scale bar:10um)

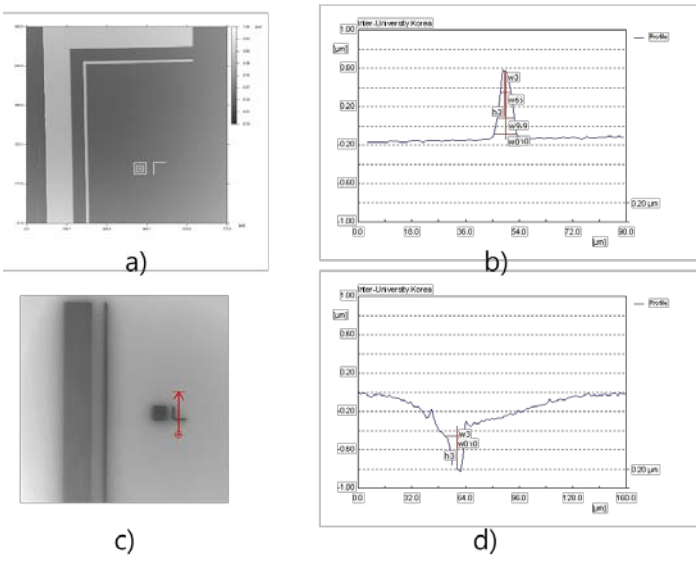

Figure 4.6 (a) Picture of nickel stamp from 3D profiler, (b) is thickness measurement of micro patterning of nickel stamper, (c) Picture of patterned film from 3D profiler, (d) is thickness of micro patterning of patterned film.

4.1.3 Solvent Bonding for Microfluidic Channel Formation

Bonding techniques are of fundamental importance in the fabrication of thermoplastic microfluidic chips. In this study, solvent bonding method was used.

A mixture of ethylene dichloride and ethanol was used as an azeotropic solvent. An azeotrope is a mixture in which the ratio of constituents in the vapor phase is equal to the ratio in the liquid phase upon boiling. In the case of ethylene dichloride and ethanol, the azeotrope possesses a characteristic boiling point below that of either individual component in the mixture. The ethylene dichloride acted as a solvent for the PMMA to PC (polycarbonate), while the ethanol served to prevent microchannel clogging. Because the composition of the solvent mixture remains unchanged during evaporation, the constant ratio of ethanol ensured that channel deformation was avoided during the drying process.

The organic solvents used in this study, i.e. acetone and ethyl alcohol are both electronic grade solvents, while 1,2-dichloroethane is DNA synthesis grade (Sigma Aldrich, USA). (*Caution*: The organic solvents are highly flammable and volatile. The bonding process must therefore be performed using a chemical hood.) The bonding solvent is composed of 20% (by weight) 1,2- dichloroethane and 80%

ethanol [71]. Note that the user can adjust the composition of the bonding solvent as required to accommodate different types of PMMA sheets with differing molecular weights and degrees of polymerization.

Fig. 4.6 presents a process of the proposed bonding method for PMMA film to PC microfluidic chips. As shown, the bonding procedure involves just three steps. Initially, PMMA film is lied on the align jig. In the second step, 20ul of bonding solvent are applied onto the contact surfaces of PMMA film. Note that the solvent is spread evenly over all of the contact surface area in order to ensure a uniform and sound bonding. Finally, upper PC chip is sandwiched and clamped in bonding machine under an applied pressure of approximately 500kPa for 4 min at 35°C. The clamping is then released and the residual solvent removed from the sealed micro channel in the dry chamber. The complete bonding process requires less than 5 min. After bonding of microfluidic chip and focus marked film, bonded chip was treated with plasma to generate hydrophilic surface. Plasma processing was chosen for this application because it is a well-established technique for surface modification. Bonded chip was treated for 1min, 750mtorr and 100W power.

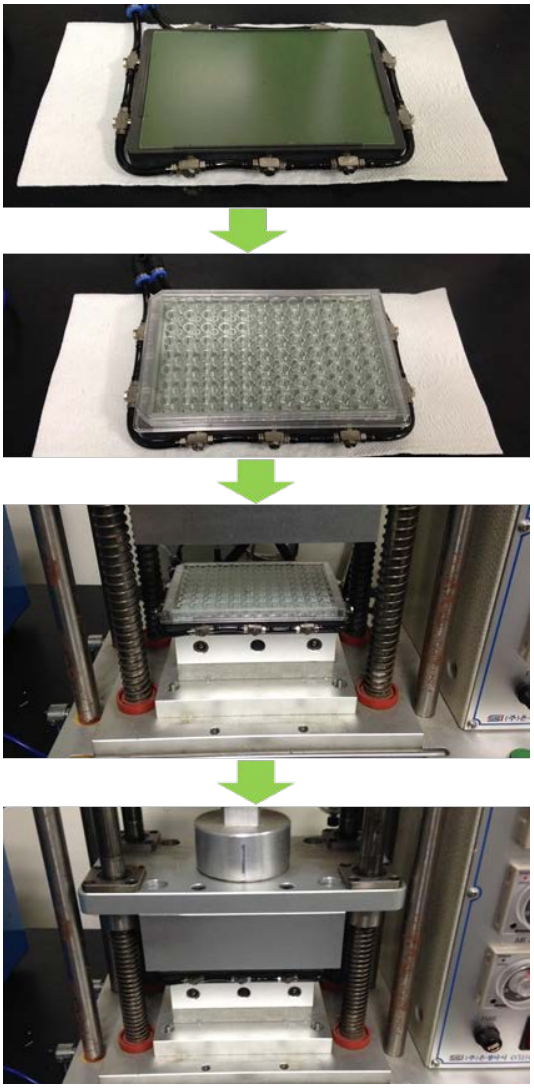

Figure 4.7 Plastic chip bonding process using bonding machine, Solvent : 20% (by weight) ethylene dicloride + 80% ethanol, Bonding, Temperature : 35℃, Bonding Time : 5min, Bonding Material : MAC(Polycarbonate) + Film(PMMA)

Figure 4.8 presents image of two microfluidic devices sealed using the proposed method. The image confirm the high bonding quality of the proposed bonding technique for the sealing of microfluidic chips since there is no leakage in the microchip. Additionally, it can be seen that the bonding procedure does not reduce the transparency of the PMMA substrates. This is clearly a considerable advantage in devices designed or optical detection applications.

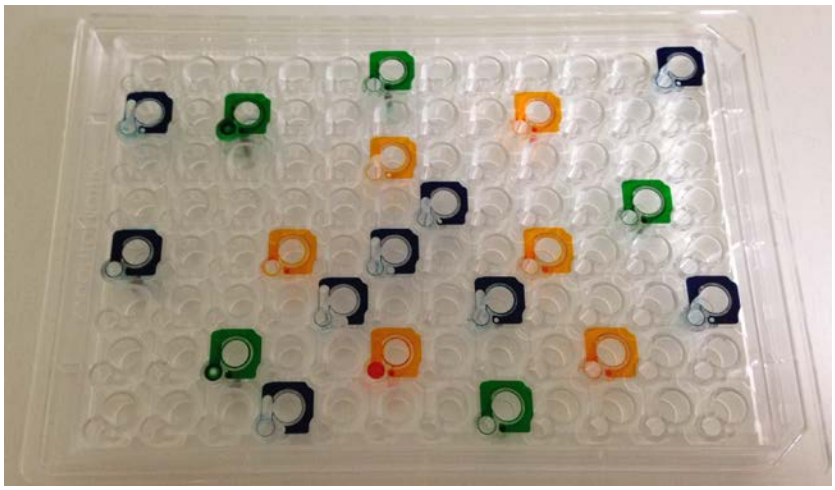

Figure 4.8 PMMA film + PC MAC chip bonding result. The image confirm the high bonding quality of the proposed bonding technique for the sealing of microfluidic chips since there is no leakage in the microchip.

4.1.5 Diffusion Characteristics in Agarose Channel

Fick's first law relates the diffusive flux to the concentration under the assumption of steady state. It postulates that the flux goes from regions of high concentration to regions of low concentration, with a magnitude that is proportional to the concentration gradient (spatial derivative). In one (spatial) dimension, the law is

$$J = D\frac{\partial C}{\partial x}$$

J : Diffusion flux(mol/cm^2s)

D : Diffusion Coefficient(cm^2/s)

C : Concentration(mol/m^3)

The diffusion coefficient of antibiotics (MW : 300~700 Da) in 0.5% agar at 37°C is about 1E-5 [72]. It depends on the concentration of agarose and temperature. We can assume the value of diffusion coefficient like Table 4.1. So, the diameter of our microfluidic channel is 500um, it takes about 1min to diffuse the channel.

J. Choi et al. used to rodamine B (fluorescence dye) to visualize and validate the diffusion characteristics of the antibiotics. Rhodamine B has a formula weight

(479.0) similar to that of amikacin (585.6), norfloxacin (319.3), tetracycline (444.4), and gentamicin (477.6). Therefore, its diffusion characteristics should be similar to those of the antibiotics. A diffusion test with rhodamine B was performed to observe its diffusion into the microchannel. Rhodamine B diffused into the imaging area where we were able to observe bacterial cell growth for 10 min. Most of the antibiotics reached the bacteria in the imaging area within a few minutes [73].

Table 4.1 Diffusion coefficient and rate of antibiotics to agarose according to the molecular weight.

MW(Da)	Diffusion Coefficient (cm^2/s)	Diffusion rate (100um)
30~70kDa	10^{-7}	1000 sec
3~7kDa	10^{-6}	100 sec
300~700Da	10^{-5}	10 sec

4.2 Optical Reader System

4.2.1 Motorized Microscopy System

For the tracking and rapid examination of single bacterial growth, motorized optical microscopy reader system including a software was developed and used in this study. For rapid antimicrobial susceptibility test, motorized optical reader system was designed. Figure 5.1 shows the system design and photography. This system consists of an inverted microscope with a charged coupled device (CCD) camera, blue LED light source, motorized x-y stage for bacteria tracking and motorized z-axis stage for autofocusing.

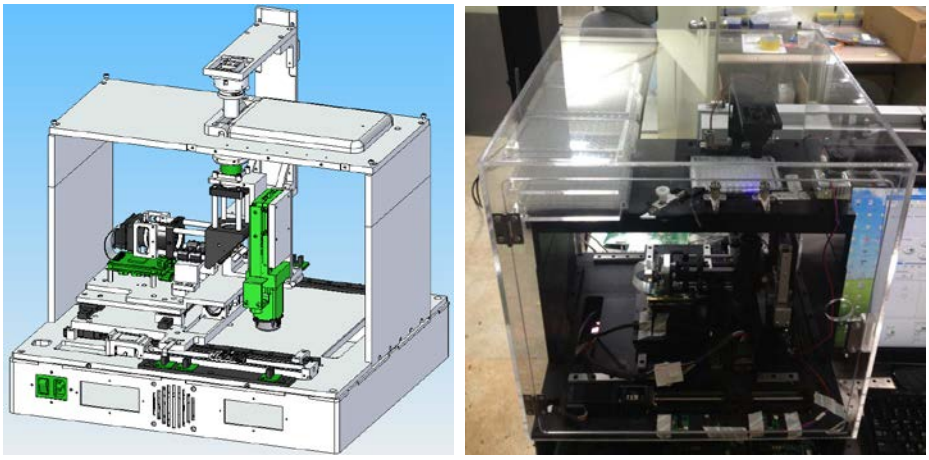

Figure 4.9 System Configuration: This system consists of an inverted microscope with a charged coupled device (CCD) camera, blue LED light source, motorized x-y and z-axis stage.

The optical components were selected for target size 1~2um, considering single bacteria size. Figure 5.2 shows designed optical microscopy part. The specifications of optical components are as follows.

- **Illumination**
    - Transmission light : 3W blue(470nm) LED, Diffuser and Prism sheet
- **Objective Lens**
    - Olympus LUCPlanFLN 20X
    - NA : 0.45
    - Long Working Distance : 10mm
    - Depth of Field : 5.8um
    - Field of View : 250 x 190 um
    - Camera Specification
- **CCD Camera**
    - Sensor : Sony ICX205
    - Type : Inter Line Transfer(ILT)
    - Resolution : 1392 x 1040 Mono
    - Pixel Pitch : 4.65um
    - Active Area : 7.6mm x 6.2mm

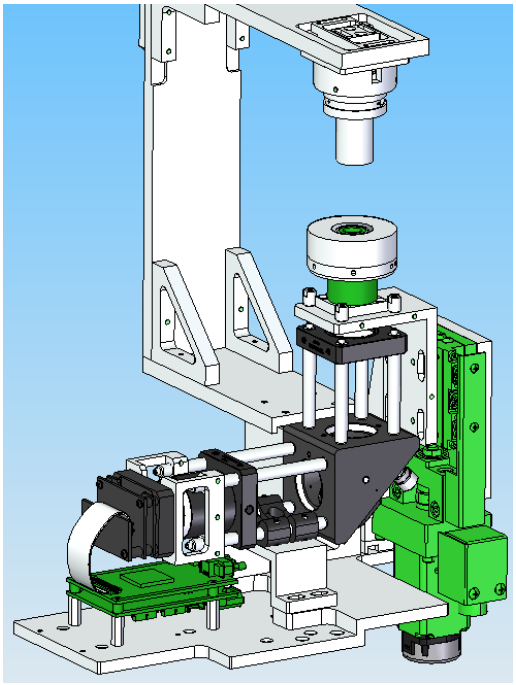

Figure 4.10 3D cad designed optical microscopy part.

Motorized XY stage was designed for automatically searching the target mark in the each well and the detection area. This stage is composed of step motor, linear actuator, and limit sensor. The specifications of XY stage are followings

- Ball screw lead Pitch : 2mm

- Travel range : 150 x 100mm

- Velocity : 10mm/s

- Load : <3kg

- 28mm stepping motor with position feedback

- Resolution : 0.036 degree

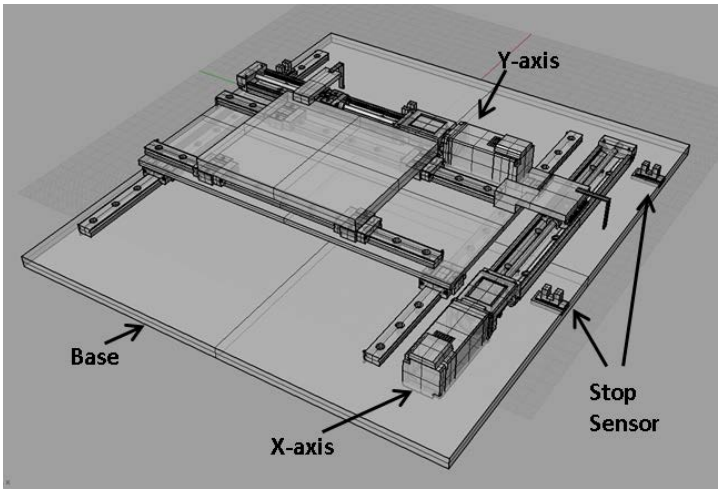

Figure 4.11 3D cad (SolidWorks) design of XY stage

To obtain the clear focus image and the shape of the image data, a appropriate objective lens for the precision drive apparatus. High-resolution micro step motor and precision backlash stage was used. Specifications are as follows.

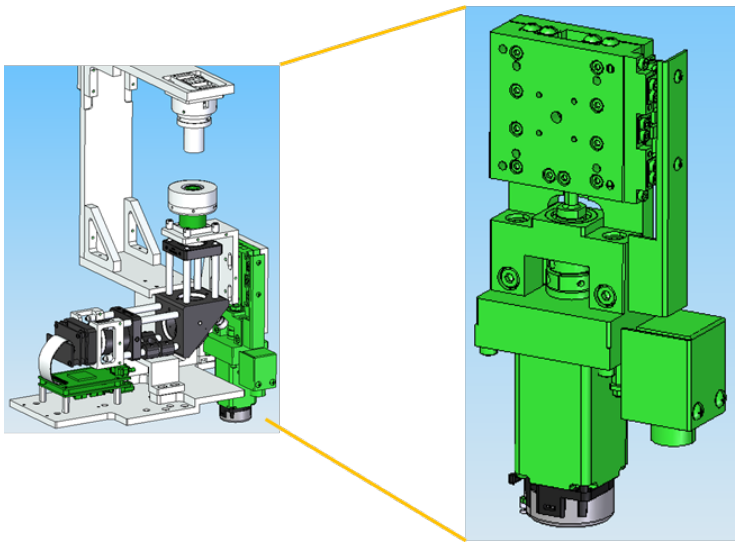

Figure 4.12 3D cad (SolidWorks) design of Z-axis stage

- Resolution : 2um/step

- Travel range : 20mm

- Speed : >5mm/s

- 1mm pitch ball screw

- 0.036 degree/step stepping motor

- Resolution : 0.1um/step

- Backlash : <0.2um

4.2.2 Software

All function of described above were controlled using LabView(National Instruments) interface in order to serve as a real measurement system. Images were captured using a black and white CCD camera with a USB interface to the computer system, and saved in 8-bit bmp. The size of the captured images was on the order of 1392 x 1040 pixels. Typical storage requirements were 1.7MB per image; images were stored to HDD for convenient archiving and retrieval.

Antibiotic Susceptibility Test for the measurement channel from the bottom of the image for the measurement of time lapse autofocusing algorithm and at the same location for each image for measurement of a focus mark, and a pattern matching centering algorithm was implemented. The flow chart of the automatic detection algorithm is shown in the Figure 4.13.

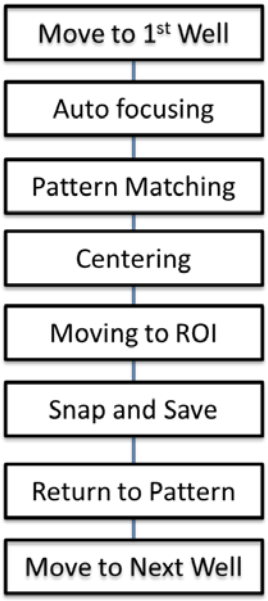

Figure 4.13 Program flow chart : Searching Initial position – Autofocusing and pattern matching of focusing mark – Centering – Moving to the detection area and snap the sample image. – Moving to the initial position

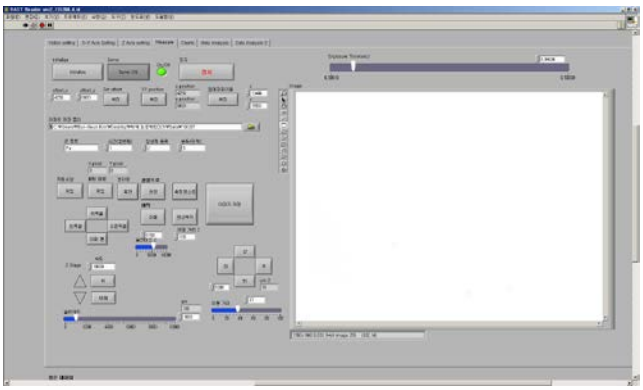

Figure 4.14 Control Software : LabView(NI, USA) interface in order to serve as a real measurement system

4.3 Rapid Antibiotic Susceptibility Test Procedure

Bacterial cells were diluted with PBS buffer and prepared from colonies overnight cultured on MHA agar plate (Final Concentration Macfaland 1.0). The bacterial cells were thoroughly mixed with 0.5% pure agarose (UltraPureTM agarose, Invitrogen) at 37℃. 10uL of the bacteria and agarose mixture was loaded into the inlet of the microfluidic channel. After solidification of the mixture, liquid medium including an antibiotic was added into the well and it was diffused into bacterial cells immobilized in or under the agarose matrix. The images of single cell growth were taken on the bottom at the interface region of the microfluidic channel at 0, 1.5 and 3 hours for Gram negative bacteria and 0, 2, 4 hours for Gram positive bacteria. The AST result was compared with the broth microdilution method recommended by Clinical and Laboratory Standards Institute (CLSI) [74].

4.4 Result and Discussion

By single cell tracking method, we could get high resolution image. The growth pattern of bacteria is different with the species and antibiotics due to the mechanism of the antibiotic to the bacteria. In this study, we established a new image method that morphological change is directly related with antimicrobial susceptibility.

The morphological changes of Gram negative bacteria in beta-lactam antibiotic condition are well studied [75], [76]. The penicillin-binding proteins (PBPs) polymerize and modify peptidoglycan, the stress-bearing component of the bacterial cell wall leading the morphological deformation. Also, the relation between the morphology and minimum inhibitory concentration is suggested by Buijs et al [77].

In the R-AST system, there were mainly two types of morphology of bacterial cell growth in antimicrobial condition, dividing (Fig 2A) and non-dividing (Fig.2 B, C and D). Dividing pattern indicates increasing number of bacterial cells (growth) and the bacterial cells had resistance to certain concentration of an antimicrobial. Non-dividing pattern was categorized into three types: No change, filament growth and cell swelling. The No change pattern was identical or negligible little growth or dividing with that of initial point and the bacterial cells were sensitive to certain concentration of an antimicrobial. The other two patterns were seen only in Gram

negative bacterial cases against beta-lactam antibiotics. Over the MIC of the antimicrobials, the bacterial cells formed only filament growth without cell division. In case of subgroup of carbapenems (meropenem and imipenem), the bacterial cells swelled and burst at longer incubation or higher concentration than MIC. In these cases, even though the volume of single cell increased, the growth was inhibited at certain point. Through these morphological data, the results of AST could be predicted. We categorized the morphologies of bacterial single cell growth under antibiotic condition and determined antibiotic sensitive or resistance by comparing the gold standard method. (Figure 4.15) Using this AST decision guideline, the AST time can be more reduced.

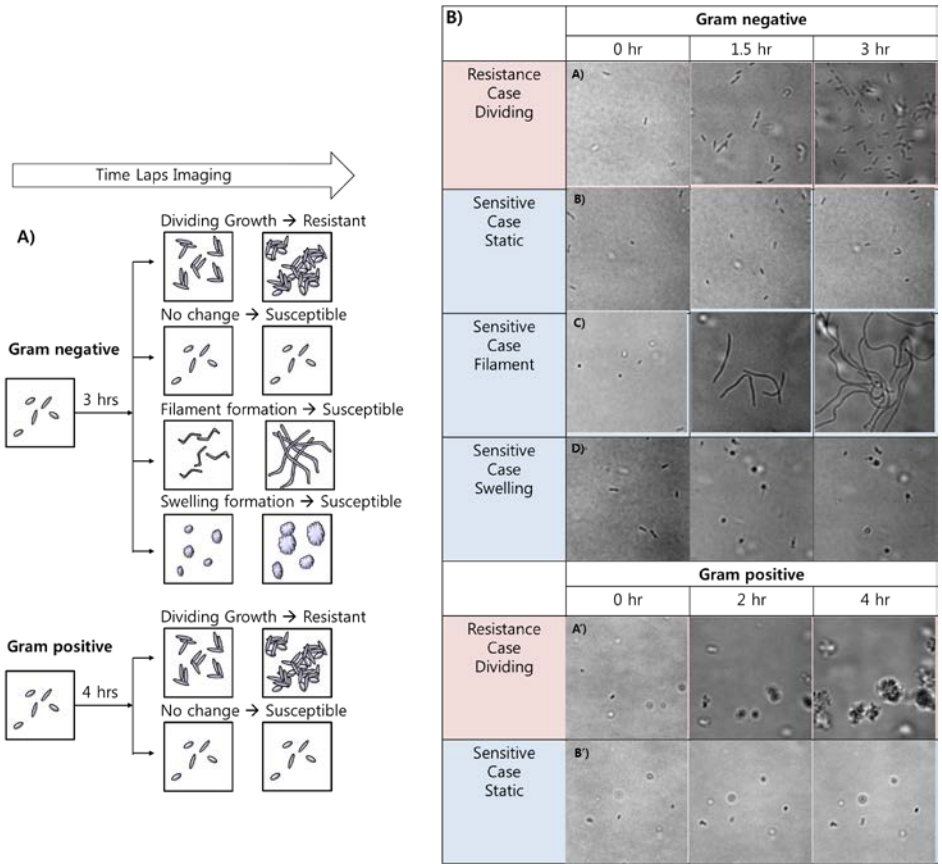

Figure 4.15 Growth patterns of bacterial cells under antibiotic treatment conditions. A and A') are common dividing types in the antibiotic-free case or the antibiotic resistance case. (A: Gram negative, A': Gram positive). B and B') are common antibiotic susceptible condition: no growth. C) is filament growth in case of Gram negative strain to beta-lactam antibiotic (susceptible). D) Swelling growth in Gram negative strain to imipenem and meropenem (susceptible).

4.4.1 Standard Strain Test

To validate the morphological determination method for R-AST, we tested 3 standard strains of CLSI (E. coli ATCC 25922, S. aureus ATCC 29213, P. aeruginosa ATCC 27853) because the strains are known as clinically important pathogens. We obtained the MIC values in 3 hours with E. coli and P. aeruginosa and 4 hours with S. aureus coinciding with the MIC range of CLSI. The antimicrobial agents were selected according to the lists of the commercial AST kits, VITEK 2 (bioMérieux, Marcy L'Étoile, France).

In P. aeruginosa and S. aureus, all cases were within the QC ranges. Figure 4.15 show the representative image for under MIC, MIC, and over MIC. Bacterial growth difference can be seen clearly. In *E.coli*, there was two cases of '5' for Imipenem and Pipericilin(Table 4.1). In case of *E.coli*, Gram negative bacteria should grow like shape of swelling under imipenem and filament under piperacilin Figure 4.16 shows the difficult case to determine the growth. In these case, detection area was out focused from the bottom. In agarose, because bacterial cell grow in a body, we cannot determine the shape whether filament or swelling

Table 4.2 Growth patterns of bacterial cells under antibiotic treatment conditions. The QC range is three values with two fold. Generally the quality control ranges are 2, 3 and 4. After obtaining images, we determined the MIC values by morphological analysis.

E. coli	항생제 농도					MIC Result	
	1	2	3	4	5	MAC	MDT
Amikacin	0.25	0.5	1	2	4	3	4
Cefepime	0.015	0.03	0.06	0.12	0.24	3	2
Imipenem	0.03	0.06	0.12	0.25	0.5	5	3
Norfloxacin	0.015	0.03	0.06	0.12	0.25	3	2
Piperacillin	0.5	1	2	4	8	5	4

P. aeruginosa	항생제 농도					MIC Result	
	1	2	3	4	5	MAC	MDT
Amikacin	0.5	1	2	4	8	3	3
Cefepime	0.25	0.5	1	2	4	3	4
Ciprofloxacin	0.12	0.25	0.5	1	2	2	3
Imipenem	0.5	1	2	4	8	2	3
Piperacillin	1	2	4	8	16	3	3

S.aureus	항생제 농도					MIC Result	
	1	2	3	4	5	MAC	MDT
Ampicillin	0.25	0.5	1	2	4	3	4
Ciprofloxacin	0.06	0.12	0.24	0.5	1	4	4
Imipenem	0.008	0.015	0.03	0.06	0.12	3	2
Oxacillin (2% NaCl)	0.06	0.125	0.25	0.5	1	4	3
Vancomycin	0.25	0.5	1	2	4	4	3

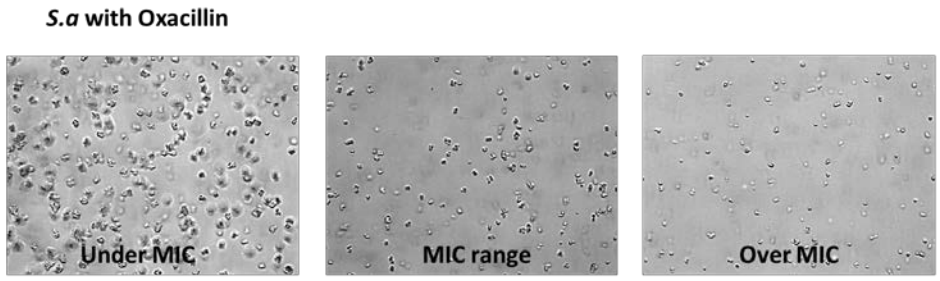

Figure 4.16 Growth patterns of bacterial cells under antibiotic treatment conditions. (*S.a* with Oxacillin : under MIC, MIC range, over MIC)

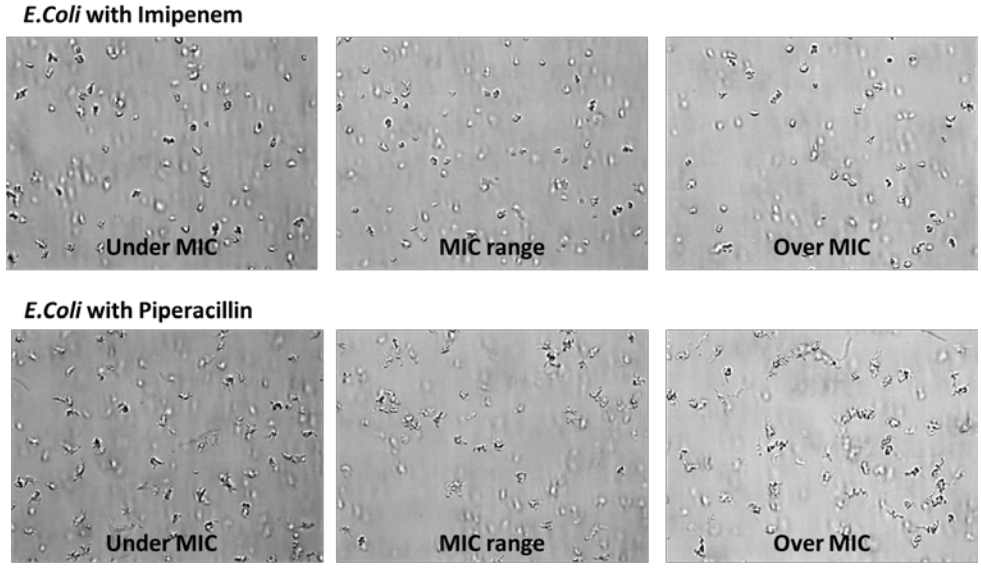

Figure 4.17 Growth patterns of bacterial cells under antibiotic treatment conditions. (*E.c* with Oxacillin : under MIC, MIC range, over MIC)

4.4.2 Clinical Sample Test

The 6 clinical samples were tested in this study. The clinical strains from various specimens (blood cultures, wound specimens, and urine) were collected from the labs of the Inchon St. Mary's Hospital (ISMH). The samples of strains from SNUH were the antibiotic resistance strains. The collection included various phenotypes with special resistance mechanisms: Prior to testing, each isolate was subcultured on cation adjusted MHA for 20~24 hours. ASTs were performed in MAC and Reader system, Vitek2 AST results were compared with the gold standard method, broth microdilution test (MDT). The image detection was automatically performed using R-AST system, and images of bacterial single cell growth are analyzed morphologically according to the MIC determination criteria established from standard strain test.

Table 4.3 Growth patterns of clinical strains under antibiotic treatment conditions. S is Susceptible, I is intermediate, R is resistance. 6 clinical sample were test. Error was occurred in *P. aeruginosa* with cefepime, piperacilin compared to mcrodilution test (MDT)

E.c												
	CLSI 항생제 농도 구간 (ug/ml) SIR range				S1				S2			
항생제	S	I		R	현미경	VITEK 2(MIC)	MDT	**Reader**	MAC 2.0	VITEK 2(MIC)	MDT	**Reader**
Amikacin	16	32		64	S	S(<=2)	S	**S**	S	S(<=2)	S	**S**
Cefepime	8	16		32	S	S(<=1)	S	**S**	I	*R,S(8)	R	**R**
Gentamicin	4	8		16	S	S(<=1)	S	**S**	R	R(>=16)	R	**R**
Imipenem	1	2		4	S	S(<=0.25)	S	**S**	S	S(<=0.25)	S	**S**

P.a												
	CLSI 항생제 농도 구간 (ug/ml) SIR range				S3				S4			
항생제	S	I		R	현미경	VITEK 2(MIC)	MDT	**Reader**	MAC 2.0	VITEK 2(MIC)	MDT	**Reader**
Amikacin	16	32		64	S	S(<=2)	S	**S**	S	S(<=2)	S	**S**
Cefepime	8	16		32	S	S(2)	I (#2 S)	**S**	S	S(<=1)	S	**S**
Imipenem	2	4		8	R(3)	R(>=16)	R	**R**	S	S(2)	S	**S**
Piperacillin	16	32	64	128	S	S(8)	R(128) (#2 13)	**S**	S	S(<=4)	S	**S**

S.a												
	CLSI 항생제 농도 구간 (ug/ml) SIR range				S5				S6			
항생제	S	I		R	현미경	VITEK 2(MIC)	MDT	**Reader**	MAC 2.0	VITEK 2(MIC)	MDT	**Reader**
Ciprofloxacin	1	2		4	I	S(<=0.5)	S	**S**	R	R(<=0.5)	R	**R**
Gentamicin	4	8		16	S	S(<=0.5)	S	**S**	R	R(<=0.5)	R	**R**
Oxacillin	2			4	S	S(>=4)	S	**S**	R	R(>=4)	R	**R**
Vancomycin	4	8	16	32	S	S(<=0.5)	S	**S**	S	S(<=0.5)	S	**S**

In error cases of gram negative strains to beta-lactam antimicrobials such as aztreonam, cefepime and imipenem, the reason of the error was owing to co-existence.(Figure 4.18) For co-existence of filament formation and dividing, we will determined this case as “resistant”.

Our morphological determination method produced accurate AST results only in 3 or 4 hours. At present, the fastest available AST platform in hospital is Vitek 2 and its average AST running time is about 9 hours excluding the sample

preparation time and some prolonged cases. Considering dairy working time (9 hours), proper antibiotics from the AST results can't be treated within the day but in the following day. The R-AST system would make the same day antibiotic treatment possible. Doern et al. reported that the rapid same-day bacterial susceptibility testing in the microbiology laboratory can have a major impact on the care and outcome of hospitalized patients with infection regarding curative value of antibiotic treatment [78].

Figure 4.18 Growth patterns of clinical sample of bacterial cells under antibiotic treatment conditions (*P.a* with Cefepime, Piperacillin : under MIC, MIC range, over MIC).

The MAC system can increase the efficiency of antibiotic treatment. If the MAC system is an automation system, the AST time can be more reduced. The morphological determination method also can contribute to reducing error rate. During AST, the bacterial single growth is monitored. If a clinical sample is contaminated by a different laboratory bacterium, it could be possible to find out and exclude this case at early stage.

Chapter 5

Conclusion

In this dissertation, a potentiometric flow cytometer capable of parallelization has been demonstrated for bacterial concentration measurement. And then, rapid antimicrobial susceptibility test system was implemented and verified. It is new method to overcome the fundamental limit of current method. Also, rapid AST can be applied to same day treatment. This proof-of-concept analysis with morphological determination offers a rapid and accurate AST results compared with existing clinically available methods.

Bibliography

[1] V. Lorian, "Some effects of subinhibitory concentrations of antibiotics on bacteria," Bulletin of the New York Academy of Medicine, 51(9), pp1046-1055, 1975.

[2] V. Soriano, AS. Perelson, F. Zoulim, "Why are there different dynamics in the selection of drug resistance in HIV and hepatitis B and C viruses?," Journal of Antimicrobial Chemotherapy 62, pp1-4, 2008.

[3] JH. Jorgensen, MJ. Ferraro, "Antimicrobial susceptibility testing: A review of general principles and contemporary practices," Clinical Infectious Diseases, 49, pp1749-1755, 2009.

[4] M. Espy, J. Uhl, L. Sloan et al.,"Real-time PCR in clinical microbiology: applications for routine laboratory testing," Clinical microbiology reviews, 19, pp165-256, 2006.

[5] J. Camara, F. Hays, "Discrimination between wild-type and ampicillin-resistant Escherichia coli by matrix-assisted laser desorption/ionization time-of-flight mass spectrometry," Analytical and Bioanalytical Chemistry, 389, pp1633-8, 2007.

[6] J. Cohen Stuart, C. Dierikx, N. Al Naiemi et al., "Rapid detection of TEM, SHV and CTX-M extended-spectrum β-lactamases in Enterobacteriaceae

using ligation-mediated amplification with microarray analysis," Journal of Antimicrobial Chemotherapy, 65, pp1377-81, 2010.

[7] JQ. Boedicker, Li L, TR. Kline, RF. Ismagilov, "Detecting bacteria and determining their susceptibility to antibiotics by stochastic confinement in nanoliter droplets using plug-based microfluidics," Lab on a Chip, 8, pp1265-72, 2008.

[8] Chen CH, Lu Y, Sin MLY, et al., "Antimicrobial susceptibility testing using high surface-to-volume ratio microchannels," Analytical Chemistry, 82, pp1012-9, 2010.

[9] Eun Y-J, Utada AS, Copeland MF, Takeuchi S, Weibel DB., "Encapsulating Bacteria in Agarose Microparticles Using Microfluidics for High-Throughput Cell Analysis and Isolation," ACS Chemical Biology, 6, pp260-6, 2010.

[10] Kim KP, Kim Y-G, Choi C-H, et al., "In situ monitoring of antibiotic susceptibility of bacterial biofilms in a microfluidic device," Lab on a Chip, 10, pp3296-9, 2010.

[11] Peitz I, van Leeuwen R., "Single-cell bacteria growth monitoring by automated DEP-facilitated image analysis," Lab on a Chip, 10, pp2944-51, 2010.

[12] Chung CC, Cheng IF, Yang WH, Chang HC., "Antibiotic susceptibility test based on the dielectrophoretic behavior of elongated Escherichia coli with

cephalexin treatment," Biomicrofluidics, 5, 021102, 2011.

[13] Sinn I, Kinnunen P, Albertson T, et al., "Asynchronous magnetic bead rotation (AMBR) biosensor in microfluidic droplets for rapid bacterial growth and susceptibility measurements," Lab on a Chip, 11, pp2604-11, 2011.

[14] Churski K, Kaminski TS, Jakiela S, et al., "Rapid screening of antibiotic toxicity in an automated microdroplet system," Lab on a Chip, 2012.

[15] Cira NJ, Ho JY, Dueck ME, Weibel DB., "A self-loading microfluidic device for determining the minimum inhibitory concentration of antibiotics," Lab on a Chip, 2012.

[16] Kalashnikov M, Lee JC, Campbell J, Sharon A, Sauer-Budge AF., "A microfluidic platform for rapid, stress-induced antibiotic susceptibility testing of Staphylococcus aureus," Lab Chip, 12, pp4523-32, 2012.

[17] Kinnunen P, McNaughton BH, Albertson T, et al., "Self-Assembled Magnetic Bead Biosensor for Measuring Bacterial Growth and Antimicrobial Susceptibility Testing," Small, 2012.

[18] Kinnunen P, Carey ME, Craig E, Brahmasandra SN, McNaughton BH., "Rapid bacterial growth and antimicrobial response using self-assembled magnetic bead sensors," Sensors and Actuators B: Chemical, 190, pp265-9, 2014.

[19] Mohan R, Mukherjee A, Sevgen SE, et al., "A multiplexed microfluidic

platform for rapid antibiotic susceptibility testing," Biosensors and Bioelectronics, 49, pp118-25, 2013.

[20] Broeren MAC, Maas Y, Retera E, Arents NLA., "Antimicrobial susceptibility testing in 90 min by bacterial cell count monitoring," Clinical Microbiology and Infection, 19, pp286-91, 2013.

[21] Fredborg M, Andersen KR, Jørgensen E. et al., "Real-Time Optical Antimicrobial Susceptibility Testing. Journal of clinical microbiology," 51,pp2047-5, 2013.

[22] Popham DL, Young KD., "Role of penicillin-binding proteins in bacterial cell morphogenesis," Current Opinion in Microbiology,6, pp594-9, 2003

[23] Biesta-Peters, E. G.; Reij, M. W.; Joosten, H.; Gorris, L. G. M.; Zwietering, M. H., " Comparison of Two Optical-Density-Based Methods and a Plate Count Method for Estimation of Growth Parameters of *Bacillus cereus*," Appl. Environ. Microbiol., 76, pp1399-1405. 2010.

[24] W.R. Hogg, W. Coulter; Apparatus and method for measuring a dividing particle size of a particulate system; United States Patent 3557352.

[25] R.W. DeBlois, C.P. Bean . "Counting and sizing of submicron particles by the resistive pulse technique". Review of Scientific Instruments 41 (7), pp909–916. 1970.

[26] Muirhead, K. A.; Horan, P. K.; Poste, G., "Flow cytometry: Present and

future," Nat. Biotechnol., 3, pp 337-356. 1985

[27] Laerum, O. D.; Farsund, T. “Clinical application of flow cytometry: a review” Cytometry, 2(1), pp1-13, 1981.

[28] Shapiro, H. M., "The evolution of cytometers," Cytometry A, 58A, 13-20. 2004.

[29] Huh, D.; Gu, W.; Kamotani, Y.,"Grotberg, J. B.; Takayama, S. “Microfluidics for flow cytometric analysis of cells and particles”, Physiol. Meas. 26, pp73-98. 2005.

[30]Chung, T. D., Kim, H. C., “Recent advances in miniaturized microfluidic flow cytometry for clinical use”, Electrophoresis, 28, pp4511-4520. 2007.

[31] Schrum, D. P., Culbertson, C. T., Jacobson, S. C., Ramsey, J. M. “Microchip Flow Cytometry Using Electrokinetic Focusing” Anal. Chem., 71, pp4173-4177. 1999.

[32] McClain, M. A., Culbertson, C. T., Jacobson, S. C., Ramsey, J. M. “Flow cytometry of Escherichia coli on microfluidic devices” Anal. Chem., 73, pp5334-5338. 2001.

[33] Fu, A. Y., Spence C., Scherer, A., Arnold, F. H. Quake, S. R., “A microfabricated fluorescence-activated cell sorter” Nat. Biotechnol., 17, pp1109-1111. 1999.

[34] Wolff, A. Perch-Nielsen, I. R. Larsen, U. D. Friis, P. Goranovic, G.; Poulsen,

C. R. Kutter, J. P. Telleman, P. “Integrating advanced functionality in a microfabricated high-throughput fluorescent-activated cell sorter” Lab Chip, 3, pp22-27, 2003.

[35] Coulter, W. H., "High speed automatic blood cell counter and cell size analyzer," Proc. Natl. Electron. Conf., 12, 1034–1040, 1956.

[36] Saleh, O.A.; Sohn, L. L. “Quantitative sensing of nanoscale colloids using a microchip Coulter counter” Rev. Sci. Instrum., 72, pp4449-4451, 2001.

[37] Satake, D.; Ebi, H.; Oku, N.; Matsuda, K.; Takao, H.; Ashiki, M.; Ishida, M., "A sensor for blood cell counter using MEMS technology," Sensor. Actuat. B, 83, pp77-81, 2002.

[38] Wood, D. K.; Oh, S.-H.; Lee, S.-H.; Soh, H. T.; Cleland, A. N. “High-bandwidth radio frequency Coulter counter”, Appl. Phys. Lett., 87, pp184106. 2005.

[39] Chun, H.; Chung, T. D.; Kim, H. C. “Cytometry and Velocimetry on a Microfluidic Chip Using Polyelectrolytic Salt Bridges” Anal. Chem., 77, pp2490-2495, 2005.

[40] Kim, K. B.; Chun, H.; Kim, H. C.; Chung, T. D. “Red blood cell quantification microfluidic chip using polyelectrolytic gel electrodes” Electrophoresis, 30, pp1464-1469, 2009.

[41] Fraikin, J.-L.; Teesalu, T.; Mckenney, C. M.; Ruoslahti, E.; Cleland, A. N., “A

high-throughput label-free nanoparticle analyser", Nat. Nanotechnol., 6, pp308-313, 2011.

[42] Roberts G. S., Kozak D., Anderson W., Broom M. F., Vogel R., Trau M. "Tunable Nano/Micropores for Particle Detection and Discrimination: scanning Ion Occlusion Spectroscopy", Small, 6, pp2653-2658. 2010.

[43] Willmott G. R., Vogel R., Yu S. S. C., Groenewegen L. G., Roberts G. S., Kozak D., Anderson W., Trau M. "Tunable Nano/Micropores for Particle Detection and Discrimination: scanning Ion Occlusion Spectroscopy", J. Phys. Condens. Matter, 22, pp454116, 2010.

[44] Vogel R., Willmott G., Kozak D., Roberts G. S., Anderson W., Groenewegen L., Glossop B., Barnet A., Turner A., Trau M., "Quantitative Sizing of Nano/Microparticles with a Tunable Elastomeric Pore Sensor", Anal. Chem., 83, pp3499-3506, 2011.

[45] Roberts, G. S.; Yu, S.; Zeng, Q.; Chan, L. C. L.; Anderson, W.; Colby, A. H.; Grinstaff, M. W.; Reid, S.; Vogel, R. "Tunable pores for measuring concentrations of synthetic and biological nanoparticle dispersions", Biosens. Bioelectron., 31, pp17-25, 2012.

[46] Vogel, R.; Anderson, W.; Eldridge, J.; Glossop, B.; Willmott, G. "A Variable Pressure Method for Characterizing Nanoparticle Surface Charge Using Pore Sensors", Anal. Chem., 84, pp3125-3131, 2012.

[47] Li, J.; Stein, D.; McMullan, C.; Branton, D.; Aziz, M. J.; Golovchenko, J. A. “Ion-beam sculpting at nanometer length scales”, Nature, 412, pp166-169, 2001.

[48] Dekker, C. ,” Solid-state nanopores”, Nat. Nanotechnol., 2, pp209-215. 2007.

[49] Clarke, J.; Wu, H.-C.; Jayasinghe, L.; Patel, A.; Reid, S.; Bayley, H., ” Continuous base identification for single-molecule nanopore DNA sequencing”, Nat. Nanotechnol., 4, 265-270, 2009.

[50] Meller, A.; Nivon, L.; Branton, D. , “Voltage-Driven DNA Translocations through a Nanopore”, Phys. Rev. Lett., 86, pp3435-3438, 2001.

[51] Ayliffe, H. E.; Frazier, A. B.; Rabbitt, R. D. J., "Electric impedance spectroscopy using microchannels with integrated metal electrodes," Microelectromech. S., 8, pp50-57, 1999.

[52] Gawad, S.; Schild, L.; Renaud, Ph. “Micromachined impedance spectroscopy flow cytometer for cell analysis and particle sizing”, Lab Chip, 1, pp76-82, 2001.

[53] Sun, T.; Holmes, D.; Gawad, S.; Green, N. G.; Morgan, H., “High speed multi-frequency impedance analysis of single particles in a microfluidic cytometer using maximum length sequences”, Lab Chip, 7, pp1034-1040, 2007.

[54] Holmes, D.; Pettigrew, D.; Reccius, C. H.; Gwyer, J. D.; van Berkel, C.;

Holloway, J.; Davies, D. E.; Morgan, H. “Leukocyte analysis and differentiation using high speed microfluidic single cell impedance cytometry”, Lab Chip, 9, pp2881-2889, 2009.

[55] Sun, T.; Morgan, H. “Single-cell microfluidic impedance cytometry: a review“, Microfluid Nanofluid, 8, pp 423-443. 2010.

[56] McKenna, B. K.; Evans, J. G.; Cheung, M. C.; Ehrlich, D. J. , “A parallel microfluidic flow cytometer for high-content screening”, Nat. Methods, 8, 401-403, 2011.

[57] Mckenna, B. K.; Selim, A. A.; Bringhurst, F. R.; Ehrlich, D. J. ,” 384-Channel parallel microfluidic cytometer for rare-cell screening”, Lab Chip, 9, pp305-310, 2009.

[58] Hur, S. C.; Tse, H. T. K.; Di Carlo, D. ,” Sheathless inertial cell ordering for extreme throughput flow cytometry”, Lab Chip, 10, pp274-280, 2010.

[59] Di Carlo, D.; Irimia, D.; Tompkins, R. G.; Toner, M. ,” Continuous inertial focusing, ordering, and separation of particles in microchannels”, Proc. Natl. Acad. Sci. U.S.A. 2007, 104, pp18892-18897, 2007.

[60] Gossett, D. R.; Di Carlo, D. , "Particle Focusing Mechanisms in Curving Confined Flows", Anal. Chem., 81, pp8459-8465, 2009

[61] Di Carlo, D. ,” Inertial microfluidics”, Lab Chip, 9, pp3038-3046, 2009

[62] Zhe, J.; Jagtiani, A.; Dutta, P.; Hu, J.; Carletta, J. J. , “A micromachined high

throughput Coulter counter for bioparticle detection and counting“, Micromech. Microeng, 17, pp304-313, 2007

[63] Jagtiani, A. V.; Zhe, J.; Hu, J.; Carletta, “Detection and counting of micro-scale particles and pollen using a multi-aperture Coulter counter”, J. Meas. Sci. Technol., 17, pp1706-1714, 2006.

[64] Jagtiani, A. V.; Carletta, J.; Zhe, J. ,” A microfluidic multichannel resistive pulse sensor using frequency division multiplexing for high throughput counting of micro particles”, J. Micromech. Microeng., 21, pp65004, 2011

[65] J. Kim, E. G. Kim, S. Bae, S. Kwon, H. Chun, "Photentiometric multichannel cytometer microchip for high-throughput microdispersion analysis", Analytical Chemistry, 85(1), pp362-368, 2013.

[66] Seaver, M.; Roselle, D. C.; Pinto, J. F.; Eversole, J. D. “Absolute Emission Spectra from Bacillus subtilis and Escherichia coli Vegetative Cells in Solution”, Appl. Optics, 37, pp5344-5347, 1998.

[67] Davey, H. M.; Kell, D. B. ,” Flow cytometry and cell sorting of heterogeneous microbial populations: The importance of single-cell analyses”, Microbiol. Rev., 60, pp641-696, 1996.

[68] Steen, H. B. ,” Flow cytometry of bacteria: glimpses from the past with a view to the future”, J. Microbiol. Meth., 42, pp65-74, 2000.

[69] Cho H, Kim H-Y, Kang JY, Kim TS. How the capillary burst microvalve

works. Journal of Colloid and Interface Science, pp306:379-85, 2007.

[70] Huang CP, Lu J, Seon H, et al. Engineering microscale cellular niches for three-dimensional multicellular co-cultures. Lab Chip, 9, pp1740-8, 2009

[71] C.Lin, C.H.Chao, C.W.Lan, " Low azeotropic solvent for bonding of PMMA microfluidic devices", Sensors and Actuators B, 121, pp698-705, 2007.

[72] D.F.Stickle, Douglas A.L, S.H.Zigmond, "Measurement of chemoattractant concentration profiles and diffusion coefficient in agarose", Journal of Immunological Methods, 70, pp65-74, 1984.

[73] J.Choi, Y.G.Jung, J.Kim, S.Kim, Y.Jung, H.Na, S.Kwon, " Rapid antibiotic susceptibility testing by tracking single cell growth in a microfluidic agarose channel system", Lab Chip, 13(2), pp 280-287, 2013.

[74] Wikler MA, Cockerill FR, Bush K, et al. Methods for dilution antimicrobial susceptibility tests for bacteria that grow aerobically: approved standard. Eighth Edition ed: Clinical and Laboratory Standards Institute, 2009.

[75] D. L. Popham, K. D. Young, "Role of penicillin-binding proteins in bacterial cell morphogenesis." Current Opinion in Microbiology, 6, pp594-599 (2003).

[76] W. Margolin, "Sculpting the bacterial cell." Current Biology, 19, pp812-822 , 2009.

[77] J. Buijs, A. S. M. Dofferhoff, J. W. Mouton, J. H. T. Wagenvoort, J. W. M. Van Der Meer, "Concentration-dependency of β-lactam-induced filament

formation in Gram-negative bacteria." Clinical Microbiology and Infection, 14, pp344-349 , 2008.

[78] Doern GV, Vautour R, Gaudet M, Levy B. "Clinical impact of rapid in vitro susceptibility testing and bacterial identification.", Journal of Clinical Microbiology , 32, pp1757-62. 1994.

국문 초록

항생제 감수성 검사는 현재 국내에서 한해 약 300 만 건 이상이 처리되고 있으며 임상 검체에서 세균 동정이 이루어지는 경우 대부분 시행된다. 특히 패혈증을 비롯한 대부분의 감염 병증에서는 반드시 항생제 감수성 검사를 시행해서 치료 효과를 높이고 항생제 내성율의 증가를 예방할 수 있는 적절한 항균 요법을 유도할 수 있도록 해야 한다. 임상적으로 감염증이 의심되는 경우 임상 검체의 추출에서부터 항생제 감수성 검사의 결과가 나오기까지 최소 3~4 일이 소요되므로 경험적 광범위 항균제 요법을 시행하고 있으나 이는 부적절한 항생제 사용으로 이어지고 결국 항생제 내성을 증가시키게 되므로 다제 내성균의 발생을 초래할 가능성이 높다. 그러므로 항생제 감수성 검사 결과를 보다 신속하게 얻는다면 경험적 항생제 처방의 횟수를 줄일 수 있어 항생제 내성을 줄이는 효과를 가져 올 수 있다. 이를 위해, 본 논문에서는 신속한 항생제 감수성 검사를 수행할 수 있는 이미지 기반의 단일 세균 분석 기술을 개발하기 위한 연구를 진행하였다.

기존의 항생제 감수성 검사 방법은 배양된 균을 흡광도를 이용하여 108/ml 개로 정량한 후에 다른 종류 및 농도의 항생제가 들어있는 각각의 웰에 접종함으로써 시작된다. 샘플이 접종된 웰 플레이트를 약 18 시간 정도 배양한 후에 흡광도를 측정하게 되는데 균이 자라는 웰은 뿌옇게 변하게 되고 항생제에 의해 균이 자라지 않는 웰은 투명하기 때문에 이를 보고 감수성 결과를 판단한다. 실제 임상 검체를 처리하는 병원에서는 이러한 방법이 자동화된 장비를 사용하고 있으며 현재 가장 많이 쓰이고 있는 장비에서는 흡광도를 시간별로 측정하여 흡광도의 변화율을 계산하는 방법으로 항생제 감수성 검사 결과를 좀 더 빠르게 제시하고 있지만 10 시간 이상이 소요되며 좀 더 신속한 결과가 요구되는 실정이다.

본 연구에서는 신속한 항생제 감수성 검사 시스템을 구현하였으며 이를 구현하기 위한 다음 기술들이 개발되었다. 미세 유체관의 좁은 영역을 통과하는 단일 세균에 의해 변하는 전기 저항을 이용하여 균을 계수함으로써 작은 농도의 균의 수도 정확히 측정할 수 있는 기술과 항생제에 대한 균의 반응을 관찰하기에 용이한 미세유체 기반의 바이오칩 개발 기술, 그리고 1um 정도의 크기의 세균을 정밀하게 측정 및 분석 할 수 있는 자동화된 광학 현미경 및 소프트웨어 개발 기술에 대해 소개한다. 또한 개발된 시스템을 이용하여 Clinical Laboratory Standard Institute 에서 제시하는 표준 균주 및 항생제에

대한 검증을 하였고 실제 임상 검체로부터 항생제 감수성 검사를 실시하였으며 기존 방법 대비 50% 신속한 검사를 수행하였다.

본 연구를 통해 개발된 단일 세균 분석 기반의 신속한 항생제 감수성 검사 기술은 이미지 분석 방법을 통하여 항생제 감수성 검사를 신속하게 수행하였을 뿐 아니라 다양한 균의 성장을 세밀히 관찰 할 수 있었으며 균의 다양한 이질성에 대한 연구 가능성도 제시할 수 있었다. 또한 기술이 상용화 된다면 시급한 치료를 요하는 세균성 패혈증과 같은 감염증에 대해 기존 검사 시스템 보다 빠른 진단과 조기 대응이 가능하도록 할 수 있으며 현재 대한민국에 만연해 있는 항생제 남용으로 인한 다제 내성균의 확산도 방지할 수 있을 것으로 기대 된다.

주요어 : 항생제 감수성 검사, 세균 계수, 미세 유체관, 광학 측정 시스템, 임상 시험

학번 : 2010-30977